



## Timing and climatic drivers for glaciation across monsoon-influenced regions of the Himalayan–Tibetan orogen



Madhav K. Murari<sup>a,\*</sup>, Lewis A. Owen<sup>a</sup>, Jason M. Dortch<sup>b</sup>, Marc W. Caffee<sup>c</sup>, Craig Dietsch<sup>a</sup>, Markus Fuchs<sup>d</sup>, William C. Haneberg<sup>e</sup>, Milap C. Sharma<sup>f</sup>, Amy Townsend-Small<sup>a</sup>

<sup>a</sup> Department of Geology, University of Cincinnati, Cincinnati, OH 45221, USA

<sup>b</sup> School of Environment and Development, The University of Manchester, M0 1QD, UK

<sup>c</sup> Department of Physics/PRIME Laboratory, Purdue University, West Lafayette, IN 47906, USA

<sup>d</sup> Department of Geography, Senckenbergstr. 1, Justus-Liebig-University Giessen, D-35390 Giessen, Germany

<sup>e</sup> Fugro GeoConsulting, Inc., 6100 Hillcroft, Houston, TX 77081, USA

<sup>f</sup> Centre for the Study of Regional Development, Jawaharlal Nehru University, New Delhi 110067, India

### ARTICLE INFO

#### Article history:

Received 14 November 2013

Received in revised form

17 January 2014

Accepted 21 January 2014

Available online

#### Keywords:

Garhwal

Terrestrial cosmogenic nuclides

Glacial geomorphology

Himalaya

Tibet

Asian monsoon

Mid-latitude westerlies

### ABSTRACT

Mapping and thirty-eight <sup>10</sup>Be terrestrial cosmogenic nuclide (TCN) ages help define the timing of glaciation in the monsoon-influenced Greater Himalaya in central Garhwal, India. Glacial landforms in central Garhwal are present only within a few kilometers of the present glaciers and all date to less than ~12.5 ka. This suggests that the Lateglacial and/or Holocene glacial advances were more extensive than their predecessors and hence destroyed or buried evidence for earlier glaciation or that other processes, such as intensive fluvial erosion and/or hillslope mass movements, have destroyed evidence of earlier glaciation. Prominent laterofrontal moraines date to the Lateglacial, the Early Holocene, and the Neoglaciation. Moraines next to the active ice and boulders on contemporary glaciers date to 10<sup>1</sup>–10<sup>2</sup> years before present. This suggests only a minor glacial advance during the Little Ice Age occurred in central Garhwal. These young ages indicate that inheritance of TCNs in areas that were recently glaciated is very small and likely has little effect when considering TCN ages on moraines older than the global Last Glacial Maximum. The new <sup>10</sup>Be ages are combined with 1081 recalculated <sup>10</sup>Be ages from previous studies to develop a regional framework of glaciation across the monsoon-influenced and adjacent regions of the Himalayan–Tibetan orogen. We separate what appears to be continuous glaciation into 27 regional glacial stages (plus 2 tentative glacial stages) that are termed monsoonal Himalayan–Tibetan stages (MOHITS). The regional glacial stages cover a wide chronologic range that includes: five regional glacial stages older than the Last Glacial cycle (MOHITS 13 at 483 ± 38 ka to MOHITS 5E at 122 ± 15 ka); thirteen regional glacial stages within the Last Glacial cycle (MOHITS 5B at 91 ± 15 ka to MOHITS 2A at 12.9 ± 0.9 ka); and eleven regional glacial stages during the Holocene (MOHITS 1k at 11.4 ± 0.7 ka to MOHITS 1A at 0.4 ± 0.1 ka). There are strong correlations both with periods of strong monsoons, and northern hemisphere events throughout the entire chronologic range with 16 stages linked to the monsoon, 11 stages linked to the mid-latitude westerlies, and two unassigned because of large age uncertainties. Overall, we see a complex pattern of glaciation influenced by two climatic systems throughout the mid/late Quaternary.

© 2014 Elsevier Ltd. All rights reserved.

### 1. Introduction

Glaciation in the Himalayan–Tibetan orogen likely affects both regional and global climate and may influence on the development of mountain topography (Molnar and England, 1990; Brozović et al., 1997; Zietler et al., 2001; Korup and Montgomery, 2008; Norton

et al., 2010). The extent and timing of Quaternary glaciation throughout the Himalayan–Tibetan orogen has been the focus of numerous scientific investigations during the past few decades (Lehmkuhl and Owen, 2005; Owen et al., 2005, 2008, 2012; Owen, 2009; Owen and Dortch, 2014 and references therein). Numerous studies utilizing surface exposure methods indicate complicated patterns of glaciation throughout the Himalayan–Tibetan orogen (Owen and Dortch, 2014). In the more arid regions of the orogen (<500 mm yr<sup>-1</sup> precipitation) glaciation is restricted in extent and moraine successions date back to several hundreds of thousands of

\* Corresponding author.

E-mail address: [murarimk@uc.edu](mailto:murarimk@uc.edu) (M.K. Murari).

years. In contrast, wetter monsoonal-influenced regions typically have more extensive glacial advances with little evidence preserved for glaciation older than a few tens of thousands of years.

Correlating glacial advances between and within mountain ranges is challenging because glaciation can be asynchronous due to variability of topography and the main climatic systems in the region: for the Himalayan–Tibetan orogen, these are the south Asian monsoon and the mid-latitude westerlies (Benn and Owen, 1998; Owen and Dortch, 2014). Developing robust correlations has been difficult because few numerical ages exist and those that do exist have large uncertainties (Owen and Dortch, 2014).

Using 692 published  $^{10}\text{Be}$  exposure ages, Dortch et al. (2013) developed a regional framework for glaciation across the semi-arid regions of the Greater Himalaya, Transhimalaya, and Pamir at the western end of the Himalayan–Tibetan orogen. Dortch et al. (2013) recognized sixteen regional glacial stages, the semi-arid western Himalayan–Tibetan stages (SWHTS). Using the methods of Dortch et al. (2013), we develop a regional framework for the monsoon-influenced and adjacent regions of the Himalayan–Tibetan orogen. We recalculate all published  $^{10}\text{Be}$  ages ( $n = 1081$ ) for the region and supplement this with a new chronology ( $n = 38$ ) that we develop for the southern slopes of the Greater Himalaya in central Garhwal of northern India. This new study area helps illustrate the complexity of evaluating  $^{10}\text{Be}$  data and helps characterize the nature and pattern of glaciation in one of the wetter areas of the Himalayan–Tibetan orogen.

## 2. Study areas

Our regional study spans the monsoon-influenced and adjacent mountains of the Greater Himalaya from northern Pakistan through northern India, Nepal, and southern, southeastern, eastern, and northeastern Tibet, and the easternmost Tien Shan (Fig. 1). Included are the ranges of the Greater Himalaya (Swat, Nanga Parbat, Garhwal, Nanda Devi, Annapurna, Forkha, Ganesh Himal, Langtang, and Kanchenjunga), Nyainqentanggula, Gangigabu Shan, Shululi, Gongga Shan, Hengduan Mountains, Nianbaoyeze, Bayan Har, Anyemaqen, Kunlun, Qilian Shan, and Easternmost Tien Shan (Fig. 1).

We do not include the semi-arid western Himalayan–Tibetan regions previously considered in Dortch et al. (2013).

The topography of the Himalayan–Tibetan orogen is the result of the continued collision of the Indian and Asian continental lithospheric plates starting at  $\sim 50$  Ma (Dewey et al., 1989; Yin and Harrison, 2000). The topography rises from the forelands of the orogen at a few hundred meters above sea level to the world's highest mountains at  $>8000$  m above sea level (asl). The orogen is one of the most glaciated outside of the polar realms. The climate of the region is influenced by both the mid-latitude westerlies and south Asian monsoon, with strong south–north and east–west precipitation gradients (Benn and Owen, 1998, Fig. 2). The region is drained by the Indus, Ganges, Brahmaputra, Irrawaddy, Yangtze, and Yellow Rivers.

We develop a new glacial chronostratigraphy for the detailed study area described in this paper that includes the southern slopes of the Greater Himalaya in central Garhwal south of the peaks of Ratangri (5858 m asl), Phating Pithwara (6904 m asl), and Kedarnath (6940 m asl) (Figs. 1 and 3). The valley floors within the study area rise from  $\sim 3000$  m asl and contain glaciers that advance down to elevations  $<3800$  m asl. Contemporary glacial systems in Garhwal have been studied to the east and north of our detailed study area (Haritashya et al., 2006, 2010; Singh et al., 2006, 2007, 2008). Reconstructions of former ice extents have concentrated on the Bhagirathi valley where Sharma and Owen (1996) and Barnard et al. (2004a) used OSL and TCN methods to date moraines. The region is influenced by the southwest Indian monsoon and receives much of its precipitation as monsoonal rain (probably 50–60%) from June to September, and snowfall from November to May. There are no meteorological stations in the new study area so local climate statistics are not available, but annual precipitation is estimated to be  $>1500$  mm by comparison to data for the Gangotri region to the north (Sharma and Owen, 1996) and TRMM Precipitation (PR)/TRMM Microwave Imager TM1 data (Bookhagen and Burbank, 2010). There is considerable microclimatic variation with altitude and aspect within and between valleys. The main flora in the region include *Quercus incana*, *Rhododendron arboreum*, *Pieris ovalifolia*, *Cedrus deodara*, which are tolerant to long-lying snow

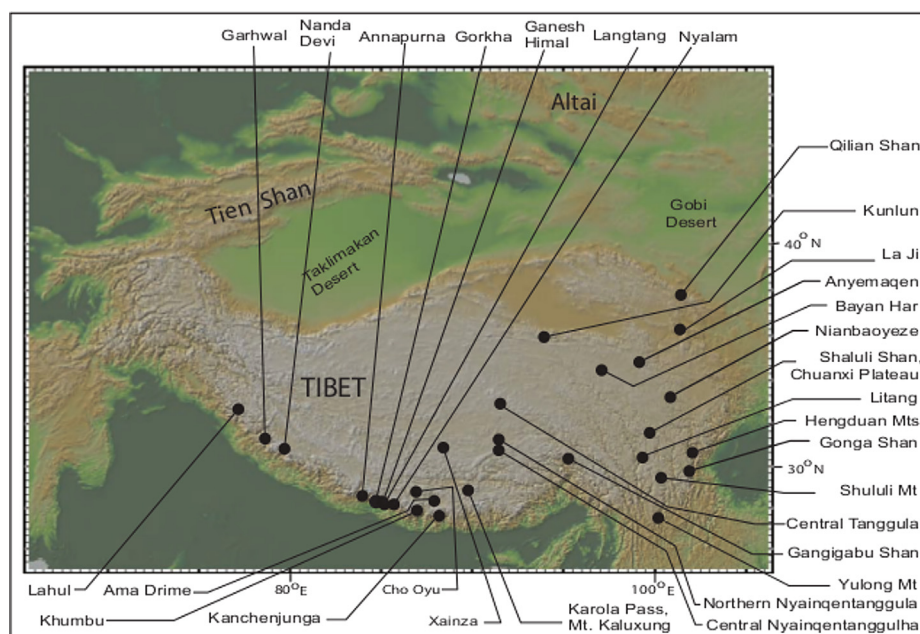
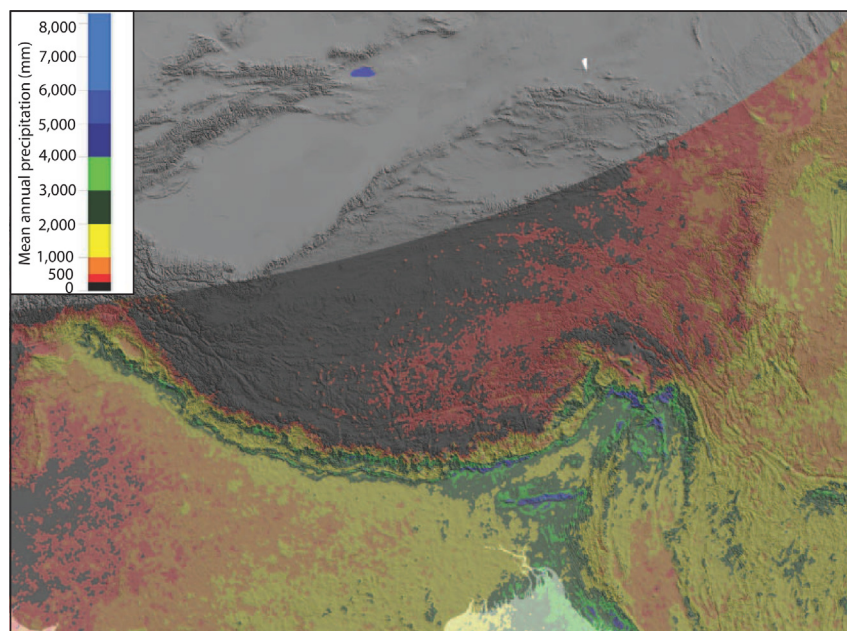


Fig. 1. Digital shaded relief image (derived from GeoMapApp) of the Himalayan–Tibetan orogen showing areas within the monsoon-influence region where the glacial geology has been described and  $^{10}\text{Be}$  dating has been undertaken in previous studies.



**Fig. 2.** Mean annual precipitation (in mm) averaged over 12 years (1998–2009) from TRMM data draped over a DEM with 36% opacity. The map was produced from data product 2B31, a combined Precipitation Radar (PR)/TRMM Microwave Imager (TMI) rain-rate product with path-integrated attenuation at 4 km horizontal and 250 m vertical resolutions (Bookhagen and Burbank, 2006, 2010; <http://www.geog.ucsb.edu/~bodo/TRMM/>). The white dots show the study areas examined in our regional analysis.

cover, and *Artemisia maritima*, *Pinus excelsa*, *Pinus geradiana*, and *Betula utilis* which occur as pioneers on scree, rock, and steep slopes (Schweinfurth, 1968). The treeline in Garhwal is represented by *B. utilis* at an altitude of ~4150 m asl (Sharma and Owen, 1996).

### 3. Methods

#### 3.1. Field methods

Two major N–S valleys, the Bhillangana and Mandakini, that traverse the southern slopes of the Greater Himalaya in central Garhwal and are connected by the Mayali Pass, were examined during a two-week trek across the region (Fig. 3). These valleys included three detailed study areas: 1) the upper Bhillangana and Dudhganga valleys; 2) the Mayali Pass valley; and 3) the Kedarnath in the upper Mandakini valley (Figs. 3 and 4). All landforms were mapped in the field with the aid of Google Earth imagery (Fig. 4).

#### 3.2. Morphostratigraphy

We follow the methods of Dortch et al. (2013) that are discussed in detail by Owen et al. (1998, 2009, 2010, 2012), Hughes et al. (2005), and Seong et al. (2009) to develop a morphostratigraphy and hence a glacial chronostratigraphy for our study areas in Garhwal. This approach includes mapping glacial and associated landforms based on their relative (morphostratigraphic) positions and relationships, and the relative weathering of their forms and surfaces. Moraines (m) were assigned a number (1 being oldest) based on their morphostratigraphic position and relative weathering characteristics, and were also assigned a letter based on the name of the study area (bd = upper Bhillangana and Dudhganga valleys; m = Mayali Pass valley; k = Kedarnath). Under this scheme, m<sub>bd1</sub> would be the oldest moraine in the upper Bhillangana–Dudhganga valleys. This morphostratigraphic approach provided a framework for sampling boulders for TCN dating as outlined in Owen et al. (1998, 2012), Seong et al. (2009), and Dortch et al.

(2013). As in these studies, a chronostratigraphy was established after numerical ages were determined for the landforms.

#### 3.3. <sup>10</sup>Be dating

Selected boulders on moraines and glacially eroded bedrock were sampled for <sup>10</sup>Be surface exposure dating by removing ~500 g of rock from the top few centimeters of the boulder or bedrock surface using a hammer and chisel. Topographic shielding was estimated using a handheld inclinometer at 15° azimuth intervals.

Quartz isolation, dissolution, chromatography, isolation of Be, and preparation of BeO were undertaken in the geochronology laboratories at the University of Cincinnati following the methods of Kohl and Nishiizumi (1992) as described in detail by Dortch et al. (2009, 2013). Ratios of <sup>10</sup>Be/<sup>9</sup>Be were measured using accelerator mass spectrometry at the Purdue Rare Isotope Measurement Laboratory at Purdue University (Supplementary item – Appendix 1).

As in Dortch et al. (2013), all ages were calculated using the CRONUS-Earth online calculator Version 2.2, which incorporates the appropriate <sup>10</sup>Be standardizations (Balco et al., 2008; Supplementary item – Appendix 1). Dortch et al. (2013) and Owen and Dortch (2014) discuss the problems associated with defining <sup>10</sup>Be ages using different scaling models and uncertainties that are associated with correcting for geomagnetic variation. We follow Dortch et al. (2013) and report the internal and external uncertainty for the time independent scaling scheme based on Lal (1991) and Stone (2000). The same scheme is used to recalculate 1081 published <sup>10</sup>Be ages from the monsoonal and adjacent areas of the Himalayan–Tibetan orogen to allow direct comparisons to be made between our new data and published data (Aoki and Imamura, 1999; Owen et al., 2001, 2003a,b,c, 2005, 2006, 2009, 2010; Lasserre et al., 2002; Schäfer et al., 2002, 2008; Finkel et al., 2003; Tschudi et al., 2003; Abramowski, 2004; Barnard et al., 2004a,b; 2006; Mériaux et al., 2004; Chevalier et al., 2005, 2011; Pratt-Sitaula, 2005; Zech et al., 2005a, 2009; Colgan et al., 2006; Gayer et al., 2006; Wang et al., 2006, 2013; Zhou et al., 2007,

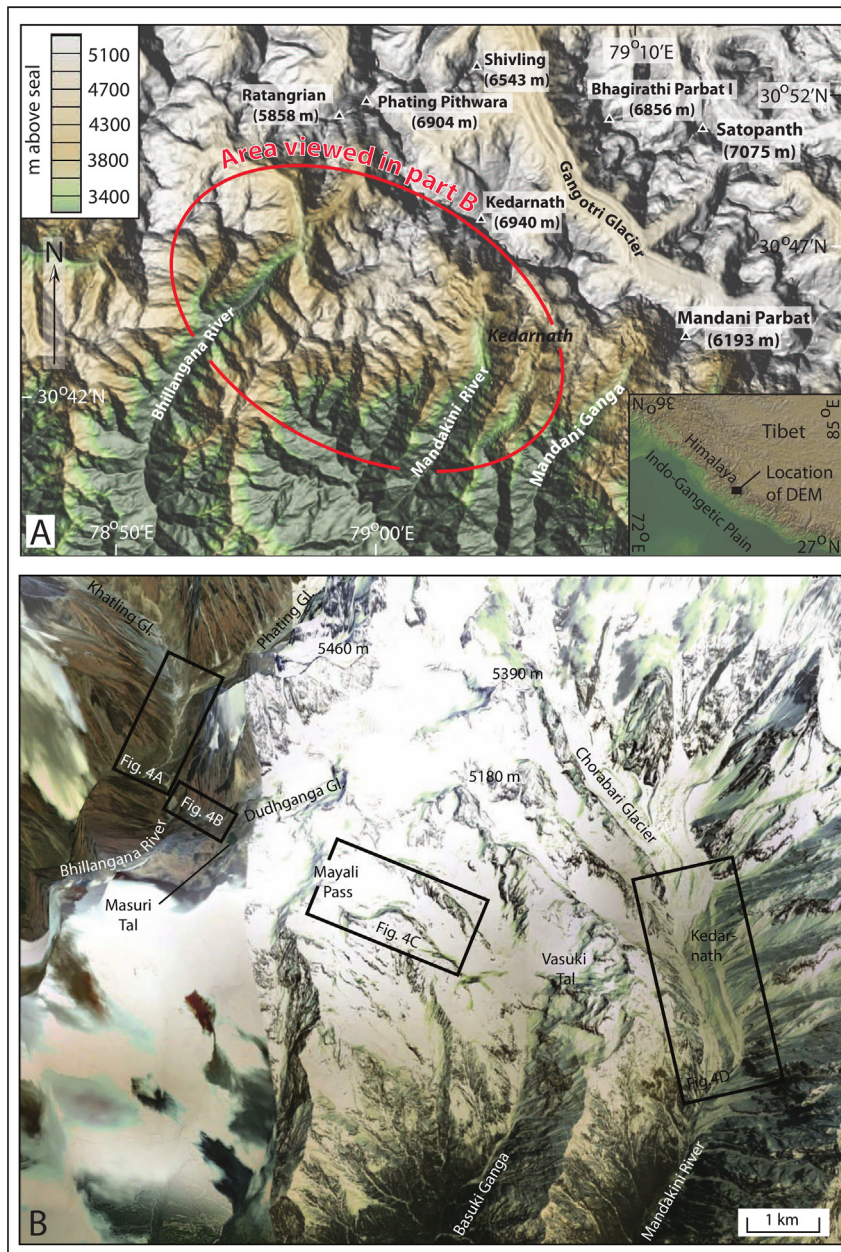


Fig. 3. (A) Location of the central Garhwal study area and (B) detailed study areas within central Garhwal on Google Earth images.

2010; Graf et al., 2008; Heimsath and McGlynn, 2008; Kong et al., 2009a,b; Strasky et al., 2009; Scherler et al., 2010; Heyman et al., 2011a; Pratt-Sitaula et al., 2011; Fu et al., 2013; Supplementary item – Appendix 1).

#### 4. Age statistics

Analysis of  $^{10}\text{Be}$  ages usually involves quantitatively describing the distribution of ages on a particular surface (e.g. Douglass et al., 2006; Ivy-Ochs et al., 2007; Chevalier et al., 2011; Heyman et al., 2011b). Dortch et al. (2013) discuss this method of analysis in more detail.

Using the methods of Dortch et al. (2013), age results from individual landforms are combined to define a local glacial stage age. Our new results are also combined with previous studies using published interpretations. Following Dortch et al. (2013), we

generate a composite probability density functions (PDFs) using the “ksdensity” kernel in MATLAB 2011a. The model of Dortch et al. (2013) takes both the uncertainty and the distribution of the individual  $^{10}\text{Be}$  measurements into account during generation of the composite PDF. Based on the number of peaks identified in the composite PDF, we decompose the empirical PDF into one or more component PDFs using non-linear least-squares regression. We report model ages as those corresponding each component PDF peak. Uncertainty of glacial stage ages, is estimated by taking the standard deviation ( $1\sigma$ ) value of component PDFs (c.f. Dortch et al., 2013). The mean of TCN ages enclosed by a component PDF can deviate from the component PDF peak, as we assume it is a normally distributed model of potentially non-normally distributed TCN ages. An example of the methodology is provided in Appendix 2 (in Supplementary items) and individual figures for all local glacial stages are shown in a series in Appendix 3 (in

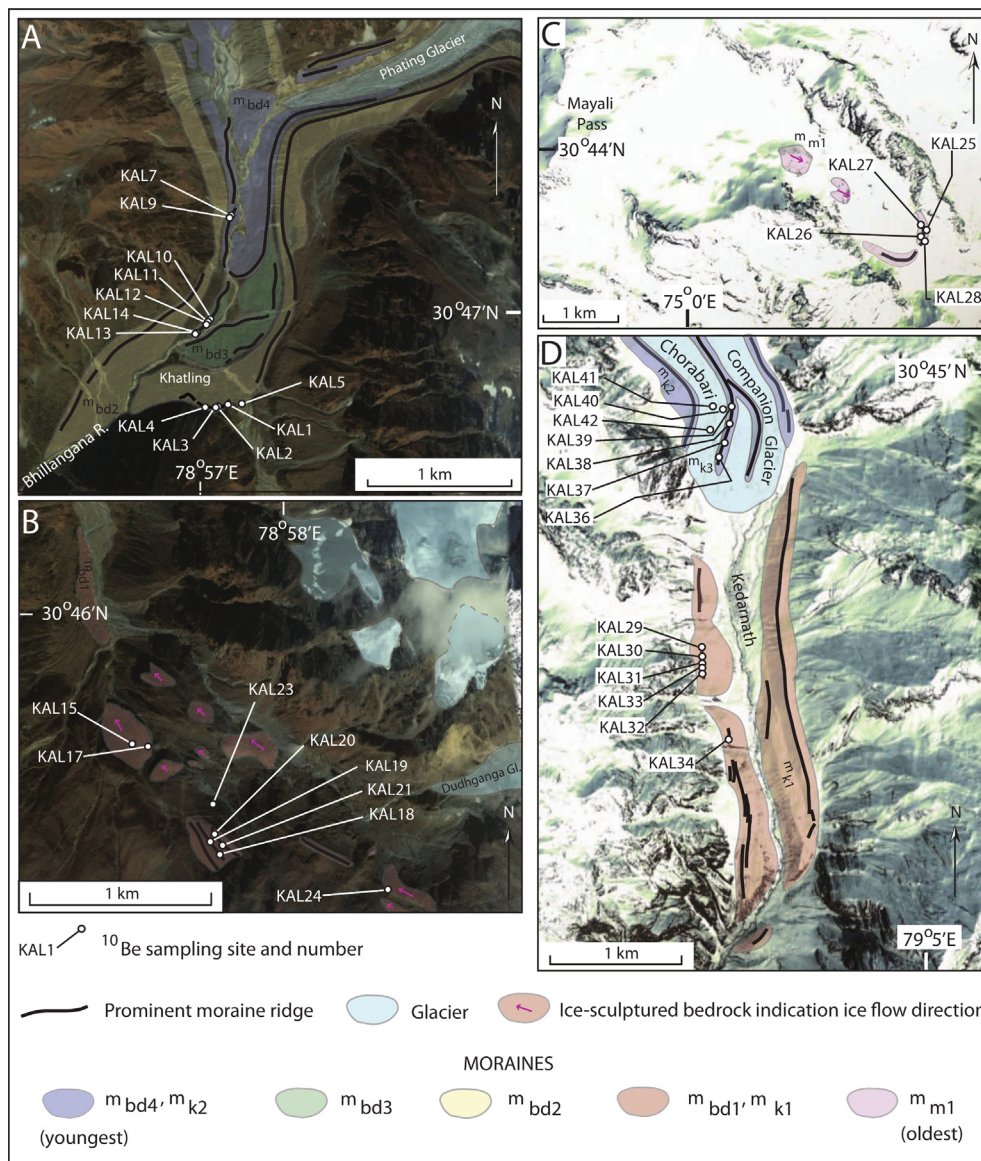


**Fig. 4.** Simplified geomorphic maps on Google Earth images of the glacial geology and sampling locations for  $^{10}\text{Be}$  dating in the detailed study areas. (A) Upper Bhillangana valley; (B) Dudhgana valley; (C) Mayali Pass valley; and (D) Kedarnath area of the upper Mandakini valley.

Supplementary items), with individual PDF plots of local glacial stages arranged in chronological order and grouped into individual files ( $n = 64$ ) based on location.

As in Dortch et al. (2013), we set the criterion that a component PDF must enclose a minimum of three ages to define a glacial stage, which is more statistically strict than many studies we reanalyzed. We consider PDFs enclosing 2 exposure ages to be tentative. This is because we recognize that a component PDF with 2 samples may be the result of under sampling. The high cost of TCN analysis influenced us to set three ages as a reasonable limit and to enclose two ages as tentative, as no study has, or will likely in the future, obtain a statistically rigorous number of samples per landform. Component PDFs containing a single age are interpreted as unreliable. In addition, we eliminate all stages that have component PDF ages with uncertainties  $\geq 50\%$  of their mean values.

Following the arguments in Dortch et al. (2013) for landforms older than 21 ka, we interpret the oldest component PDF that contains  $\geq 3$   $^{10}\text{Be}$  ages as the most likely approximation for a local glacial stage and older component PDFs with  $< 3$   $^{10}\text{Be}$  ages as

inherited outliers. This approach takes into account the possibility that moraines and individual boulders have undergone significant degradation over time. In contrast, as in Dortch et al. (2013), if two or more components are separated from the composite PDF, we take the component PDF with the highest relative probability as the best approximation of the local glacial stage age for moraines younger than 21 ka. This approach excludes samples with a few thousand years of inheritance as well as boulders that have experienced some degree of erosion or instability. We recognize that this method is more robust on larger sample numbers, but even for the small numbers of samples available to us it reduces bias in assigning ages to glacial stages. We discuss the pattern of isolated outliers at the end of the discussion as a test of our approach.

#### 4.1. Regional glacial stages

The ages of local glacial stages were examined and grouped statistically. We follow the methods of Dortch et al. (2013) by comparing the  $^{10}\text{Be}$  ages enclosed by the chosen component PDFs

using Student's *t*-test to determine if the different local glacial stages are distinct ( $p$ -value of  $\leq 0.05$ ), or if they potentially belong to the same distribution ( $p$ -value of  $> 0.05$ ). The  $^{10}\text{Be}$  ages from local glacial stages that could be part of a single normal distribution were combined to form a regional glacial stage dataset, which we call monsoonal Himalayan–Tibetan stages (MOHITS). The regional stage datasets were then compared using Student's *t*-test a second time. As in Dortch et al. (2013), all of the regional glacial stage clusters presented here have  $p$ -values of  $\leq 0.01$  (i.e., they are distinct groupings at a  $\geq 99\%$  confidence level) except for MOHITS with a  $p$ -value of 0.02, which is distinguished at a  $> 98\%$  confidence level. Regional glacial stage ages are defined using the mean and mean absolute deviation (MAD) of the combined pool of individual  $^{10}\text{Be}$  ages. Dortch et al. (2013) suggested that MAD is the preferred estimator of error as absolute deviations from the mean provide increased robustness in dealing with outliers, non-normal distributions, and comparison between groups with differing degrees of uncertainty ( $1\sigma$  values).

## 5. Landform description in central Garhwal study areas

### 5.1. Upper Billangana and Dudhganga valleys

Four distinct sets of glacial landforms are present in the upper Billangana and Dudhganga valleys (Fig. 4A and B). The oldest landforms are preserved in the Dudhganga valley and comprise glacially eroded bedrock surfaces with well-developed whaleback forms and roche moutonnées (Fig. 5A and B) and moraines (Fig. 5C and D) that we refer to as  $m_{bd1}$ . Samples for  $^{10}\text{Be}$  dating were collected from several bedrock surfaces along the valley (KAL15, 17, 23, and 24), and from a set of moraines mid-way up the valley (KAL18, 19, 20, and 21). The moraine ridges are bouldery and subdued and have a well-developed soil with peaty turf.

The next three sets of glacial landforms are preserved in the upper Billangana valley (Figs. 4A and 6A). The oldest of these,  $m_{bd2}$ , is comprised of a set of laterofrontal moraines that extend 2–3 km from the contemporary Phating and Khatling Glaciers. These moraines are steep sided ( $> 20^\circ$ ) and rise 80 m above the Bhillangana River (Figs. 4A and 6A). Boulder samples (KAL1, 2, 3, 4, and 5) were collected from the moraine crest near the mouth of the Dudhganga valley (Figs. 4A and 6C).

The next youngest set of glacial landforms comprises sharp-crested laterofrontal moraines,  $m_{bd3}$ , which rise a few tens of meters above the Bhillangana River and extend  $\sim 1.5$  km beyond the present snout of Phating Glacier (Figs. 4A and 6D). Vegetation is well developed on some of these moraines, but there are many open patches devoid of vegetation cover. Boulder samples (KAL10, 11, 12, and 13) were collected for  $^{10}\text{Be}$  dating from the crest of the westernmost moraine ridge (Figs. 4A and 5E).

The youngest set of moraines,  $m_{bd4}$ , sampled in this study area stretch from the active ice of the glaciers to  $\sim 1$  km beyond the snout of Phating Glacier (Figs. 4A and 5F). These moraines are sharp crested and have a moderate vegetation cover, but there are large areas devoid of vegetation where the moraine appears to be actively degraded. Boulder samples (KAL7 and 9) were collected for  $^{10}\text{Be}$  dating from the crest of the westernmost moraine (Figs. 4A and 5G).

### 5.2. Mayali Pass valley

The Mayali Pass valley provides access between the upper Bhillangana and Dudhganga valleys. The study area extends down valley east of the Mayali Pass (4983 m asl) for  $\sim 5$  km to a large laterofrontal moraine at  $\sim 4300$  m asl, which we named  $m_{m1}$  (Figs. 4C and 7A). This moraine has numerous m-sized boulders along its crest, but also has well developed soil and turf. Glacially eroded rock surfaces are present within the valley floor west of the laterofrontal moraines, but no younger moraines are evident. Rock glaciers are present on the northern side of the valley. Boulder samples (KAL25, 26, 27, and 28) were collected for  $^{10}\text{Be}$  dating from the crest of  $m_{m1}$  (Figs. 4C and 7B).

### 5.3. Kedarnath, Upper Mandakini valley

The Kedarnath study area is located in the upper Mandakini valley around Chorabari Glacier and its Companion Glacier (Fig. 4D). During heavy rains on 16 and 17 June 2013, moraine-dammed Chorabari Lake burst and caused devastating flooding of the Mandakini valley, washing away the towns of Kedarnath (3546 m asl), Rambara (2740 m asl), and Gaurikund (1990 m asl) (Dobhal et al., 2013). The town of Kedarnath was located on an outwash terrace south of the holy temple, Kedarnath Mandir, within two laterofrontal moraines that stretch  $\sim 3$  km down both sides of



**Fig. 5.** Landforms in the Dudhganga valley. (A) View north towards Dudhganga Glacier across glacially eroded bedrock surfaces ( $m_{bd1}$ ) from where sample KAL24 was collected. (B) Close-up view of glacially eroded surface and the sampling location for KAL17. (C) and (D) Examples of  $m_{bd1}$  moraines and sampled boulders KAL19 and KAL20.



**Fig. 6.** Landforms in the upper Billangana valley. (A) View north towards Khtaling Glacier across laterofrontal moraines  $m_{bd2}$ ,  $m_{bd3}$ , and  $m_{bd4}$ . (B) Moraine  $m_{bd2}$  and (C) typical sampled boulder (KAL5). (D) Moraine  $m_{bd3}$  and (E) typical sampled boulder (KAL11). (F) Moraine  $m_{bd4}$  and (G) typical sampled boulder (KAL7).

the Mandakini valley from Chorabari Glacier. These moraines, which we name  $m_{k1}$ , are the oldest in the study area and rise  $\sim 300$  m above the Mandakini river (Figs. 4D and 8A). The crests are prominent, rounded, and well vegetated. Samples KAL29, 30, 31, 32, 33, and 34 were collected for  $^{10}\text{Be}$  dating from the moraine crest along the western side of the valley (Figs. 4D and 8B).

A large laterofrontal moraine complex is present surrounding the snout of Chorabari Glacier. These moraines, which we call  $m_{k2}$ , rise  $\sim 100$  m from the valley floor and are sharp crested, with a sparse vegetation cover (Figs. 4D and 8C). Samples KAL36, 37, and 38 were collected for  $^{10}\text{Be}$  dating from boulders on the crest of the  $m_{k2}$  of the Chorabari Glacier (Figs. 4D and 8D).

Boulder samples KAL40, 41, and 42 were also collected for  $^{10}\text{Be}$  dating from the surface of Chorabari Glacier which we designate  $m_{k3}$ , as a check for the degree of inheritance of TCNs in supraglacial boulders (Figs. 4D, 8E and F). Although the surface of Chorabari Glacier is clearly active, with meltwater streams and small moulins, sparse patches of vegetation have developed on areas of supraglacial debris.

## 6. Results for central Garhwal

The  $^{10}\text{Be}$  ages for central Garhwal are presented graphically in Fig. 9 and in Tables 1 and 2. Fig. 9 allows us to examine the spread of



Fig. 7. View of laterofrontal moraines in the Mayali Pass valley. (A) Looking west across moraine  $m_{m1}$  and (B) typical sampled boulder (KAL26).

$^{10}\text{Be}$  ages that are less than 16 ka. The oldest moraine,  $m_{m1}$ , has  $^{10}\text{Be}$  ages that range from 11.0 to 12.5 ka, with a mean age of  $11.6 \pm 0.6$  ka (uncertainty =  $1 \sigma$ ). All ages from  $m_{m1}$  are within  $1 \sigma$  of each other providing confidence in the ages and showing that the moraine formed during the Lateglacial.

The oldest glacial landform in the Upper Bhillangana and Dudhganha valleys,  $m_{bd1}$ , yields ages that range from 0.2 to 8.8 ka. Ages of moraine boulders here are significantly younger than those for the glacially eroded surfaces, suggesting that the boulders may have been recently exhumed and/or toppled. We do not believe that the glacially eroded bedrock surfaces overestimate the ages because the deeply entrenched nature of the valley suggests many meters of glacial erosion occurred during each glacial advance, which would have exposed fresh surfaces to cosmic rays. The age for  $m_{bd1}$  based on the glacially eroded samples is  $8.3 \pm 0.4$  ka. In the Kedarnath and Upper Mandakini valley study area, the oldest moraine,  $m_{k1}$ , has ages that range from 7.4 to 14.4 ka. If sample KAL30 is excluded from the  $m_{k1}$  dataset, then the  $^{10}\text{Be}$  ages range from 7.4 to 9.1 with an average age of  $8.5 \pm 0.8$  ka. This is statistically the same age (within  $1 \sigma$ ) as the oldest glacial landforms in the Upper Bhillangana and Dudhganha valleys.

The younger moraines in the Upper Bhillangana and Dudhganha valleys have ages that range from 0.02 to 0.3 ka ( $m_{bd2}$ ), 0.2 to 2.0 ka ( $m_{bd3}$ ), and 0.05 to 0.2 ka ( $m_{bd4}$ ). The youngest ages for  $m_{bd2}$  are unrealistic and are likely due to exhumation of boulders. We therefore use the older ages to define the age of  $m_{bd2}$  to  $\sim 0.3$  ka. The ages of these three young moraines (Tables 1 and 2)

suggest that they formed during the latter part of the Neoglaciation. However, large uncertainties in the ages makes it difficult to assign them to an exact time within the Neoglaciation, except to suggest that they might represent Little Ice Age (LIA) advances.

Similarly, the large range of ages for  $m_{k2}$  in the Kedarnath and Upper Mandakini valley area makes it difficult to assign an age, except to suggest that  $m_{k2}$  formed during the later part of the Neoglaciation. Moreover, being immediately adjacent to active ice suggests that  $m_{k2}$  probably represents an LIA advance. The  $15.7 \pm 5.0$  age of sample KAL37 with its large uncertainty is clearly an outlier.

The boulder samples collected from the surface of Chorabari Glacier have  $^{10}\text{Be}$  surface exposure ages ranging from 60 to  $\sim 540$  years BP. These data suggest that there may be as much as 0.5 ka inheritance of  $^{10}\text{Be}$  in many of the moraine boulders we dated. In addition, the presence of significant outliers (e.g. samples KAL12, 13, and 37) in some of the young moraines argues for modest inheritance of TCN in moraine boulders. Such inheritance makes it challenging to assign young ages to moraines and attribute them to such times as the LIA.

In summary, our new  $^{10}\text{Be}$  ages show that glaciers advanced in central Garhwal during the Lateglacial, Early Holocene, and Neoglaciation (probably the LIA).

### 6.1. Separation of component distributions

Further examination of the new data using PDF separation shows that the datasets of glacial stages  $m_{bd2}$ ,  $m_{bd3}$ ,  $m_{bd4}$ ,  $m_{k2}$ , and  $m_{k3}$  should be excluded due to component PDFs having  $>50\%$  uncertainty in the average age (Table 2, Fig. 9). This large uncertainty is attributed to glacial landforms being unstable for a significant time after their formation as discussed by Dortch et al. (2010 and references therein) in other glaciated regions in the Himalaya, Alaska, and the Alps.

There are two component PDFs from the  $m_{m1}$  stage, the younger of which ( $11.6 \pm 0.6$  ka) encloses three ages and has the highest relative probability. The other, older component PDF is the result of a single outlier excluded from the younger PDF. This result does exemplify the potential for inherited TCNs to affect the age distribution of landforms that are global Last Glacial Maximum (gLGM) and younger in age. Two component PDFs for the  $m_{bd1}$  stage each enclose four ages but the older PDF has a significantly higher relative probability and thus defines this stage at  $8.8 \pm 4.2$  ka. The four younger ages are interpreted as exhumed or weathered boulders.

The component PDF for the  $m_{k1}$  stage ( $9.2 \pm 0.6$  ka) encloses 4 ages and excludes two outliers, one inherited and one too young. Overall the PDF separation method excludes more ages but results in similar, more robust, and typically slightly older ages than the previous method described in the section above. A complication associated with the PDF separation method makes for a larger uncertainty in the age of the  $m_{bd1}$  stage. However, this is not a limiting factor since the regional stage groupings discussed below compare statistically the enclosed ages when determining groupings, and the mean and MAD are used to define regional stages.

## 7. Regional analysis of glacial ages

Our regional synthesis of glacial chronology was undertaken by recalculating 1081 published  $^{10}\text{Be}$  ages from numerous studies throughout the monsoonal and adjacent areas of the Himalayan–Tibetan orogen (Aoki and Imamura, 1999; Owen et al., 2001, 2003a,b,c, 2005, 2006, 2009, 2010; Lasserre et al., 2002; Schäfer et al., 2002, 2008; Finkel et al., 2003; Tschudi et al., 2003;

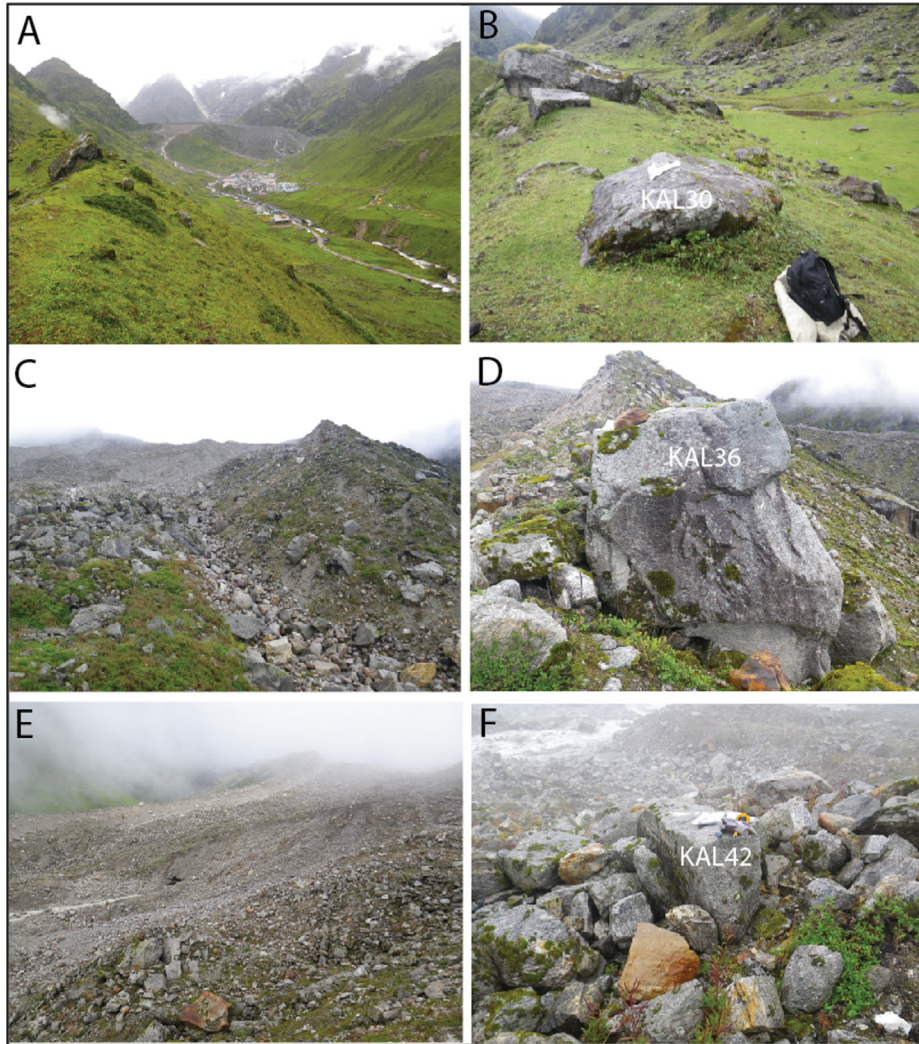


**Fig. 8.** Views of landforms in the Kedarnath area of the upper Mandakini valley. (A) View north towards Chorabari Glacier with moraine  $m_{k1}$  in the foreground. (B) Typical sampled boulder (KAL30) on the  $m_{k1}$  moraine. (C) View of laterofrontal moraine  $m_{k2}$  with Chorabari Glacier in the background, and (D) typical sampled boulder (KAL36) on  $m_{k2}$ . E) View of Chorabari Glacier from  $m_{k2}$  looking west, and F) typical sampled boulder (KAL42) on  $m_{k3}$ .

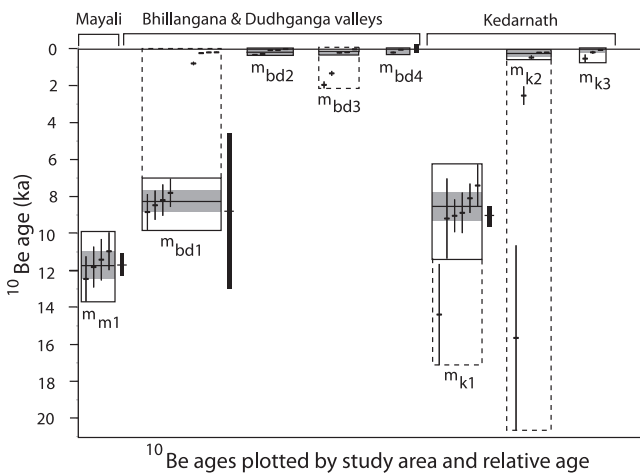


**Fig. 9.**  $^{10}\text{Be}$  ages for moraines and glacially eroded surfaces in central Garhwal plotted by area and relative age. Rectangles enclose data for individual moraines with dashed rectangles highlighting  $^{10}\text{Be}$  ages considered outliers. Solid rectangles group data with thin horizontal line showing the mean age and gray shaded bar  $1\sigma$  of the enclosed samples. The thicker black bars outside the rectangles are the component PDF ages with  $1\sigma$  uncertainty.

Abramowski, 2004; Barnard et al., 2004a,b; 2006; Mériaux et al., 2004; Chevalier et al., 2005, 2011; Pratt-Sitaula, 2005; Zech et al., 2005a, 2009; Colgan et al., 2006; Gayer et al., 2006; Wang et al., 2006, 2013; Zhou et al., 2007, 2010; Graf et al., 2008; Heimsath and McGlynn, 2008; Kong et al., 2009a,b; Strasky et al., 2009; Scherler et al., 2010; Heyman et al., 2011a; Pratt-Sitaula et al., 2011; Fu et al., 2013; Supplementary item – Appendix 1). We did not consider studies in the semi-arid western regions of the Himalayan–Tibetan orogen, which are the focus of Dortch et al. (2013). Individual graphs for all the glacial stages used are presented in Appendix 3 (in Supplementary items), which contains 63 figures arranged alphabetically by location and internally arranged in chronological order.

We assume that each valley contains a partial record of glacial advances with glaciers responding not only to regional climate, but also to numerous topographic and micro-climatic factors. Thus, an understanding of regional glaciation can be gained by combining partial individual valley records into a regional framework (Dortch et al., 2013). Where a significant and datable glacial advance occurs in more than one mountain range (i.e. ages are indistinguishable,  $p \geq 0.05$ ), we define a regional glacial stage as a monsoonal Himalayan–Tibetan stage (MOHITS). Following the approach of Dortch et al. (2013), the MOHITS numbers (1A–13) broadly correlate with Marine Oxygen Isotope Stage (MIS)

**Table 1**  
Sample numbers, descriptions, locations, <sup>10</sup>Be data, and <sup>10</sup>Be ages for glacial landforms in southern Garhwal.

Sample number	Landform type	Relative age	Boulder size height/width/length (cm)	Sample thickness <sup>a</sup> (cm)	Latitude (°N)	Longitude (°E)	Altitude <sup>b</sup> (m asl)	Topographic correction	<sup>10</sup> Be concentration <sup>c</sup> (atoms/g SiO <sub>2</sub> × 10 <sup>4</sup> )	Age Time independent Lal (1991)/Stone (2000) <sup>d</sup> (ka)	Age Desilet et al. (2003, 2006) <sup>d</sup> (ka)	Age Dunai (2001) <sup>d</sup> (ka)	Age Lifton et al. (2005) <sup>d</sup> (ka)	Age Time dependent Lal (1991)/Stone (2000) <sup>d</sup> (ka)
<b>Bhillangana and Dudhganga valleys</b>														
KAL7	Moriane ridge	m <sub>bd4</sub>	100/110/170	3	30.7898	78.9522	3635	0.911	0.68 ± 0.12	0.18 ± 0.03 (0.04)	0.22 ± 0.05	0.22 ± 0.05	0.23 ± 0.05	0.20 ± 0.04
KAL9	Moriane ridge	m <sub>bd4</sub>	70/130/150	3	30.7897	78.9523	3637	0.911	0.17 ± 0.03	0.05 ± 0.01 (0.01)	0.06 ± 0.01	0.06 ± 0.01	0.06 ± 0.01	0.05 ± 0.01
KAL10	Moriane ridge	m <sub>bd3</sub>	130/110/260	3	30.7839	78.9511	3579	0.937	0.62 ± 0.12	0.16 ± 0.03 (0.04)	0.20 ± 0.05	0.20 ± 0.05	0.21 ± 0.05	0.19 ± 0.04
KAL11	Moriane ridge	m <sub>bd3</sub>	110/220/200	2.5	30.7838	78.9509	3576	0.937	0.70 ± 0.09	0.19 ± 0.02 (0.03)	0.23 ± 0.04	0.23 ± 0.04	0.23 ± 0.04	0.21 ± 0.03
KAL12	Moriane ridge	m <sub>bd3</sub>	80/120/200	2	30.7836	78.9507	3568	0.937	4.73 ± 0.25	1.26 ± 0.07 (0.13)	1.41 ± 0.18	1.50 ± 0.19	1.42 ± 0.16	1.33 ± 0.13
KAL13	Moriane ridge	m <sub>bd3</sub>	100/130/200	3	30.7834	78.9504	3571	0.943	6.93 ± 0.32	1.84 ± 0.08 (0.18)	2.09 ± 0.27	2.25 ± 0.28	2.10 ± 0.23	1.96 ± 0.19
KAL14	Moriane ridge	m <sub>bd3</sub>	70/90/100	2.5	30.7831	78.9501	3571	0.938	1.00 ± 0.01	0.3 ± 0.003 (0.004)	0.03 ± 0.01	0.03 ± 0.01	0.03 ± 0.01	0.03 ± 0.004
KAL1	Moriane ridge	m <sub>bd2</sub>	70/120/200	1.5	30.7778	78.9515	3641	0.937	0.99 ± 0.08	0.25 ± 0.02 (0.03)	0.31 ± 0.05	0.31 ± 0.04	0.32 ± 0.04	0.29 ± 0.03
KAL2	Moriane ridge	m <sub>bd2</sub>	140/275/330	2	30.7777	78.9512	3650	0.923	1.14 ± 0.12	0.29 ± 0.03 (0.04)	0.36 ± 0.06	0.36 ± 0.06	0.37 ± 0.05	0.33 ± 0.04
KAL3	Moriane ridge	m <sub>bd2</sub>	110/150/270	1.5	30.7782	78.9506	3646	0.935	0.25 ± 0.03	0.06 ± 0.01 (0.01)	0.08 ± 0.01	0.08 ± 0.01	0.08 ± 0.01	0.07 ± 0.01
KAL4	Moriane ridge	m <sub>bd2</sub>	80/130/210	1.5	30.7782	78.9504	3657	0.923	0.05 ± 0.02	0.01 ± 0.01 (0.01)	0.02 ± 0.01	0.02 ± 0.01	0.02 ± 0.01	0.02 ± 0.01
KAL5	Moriane ridge	m <sub>bd2</sub>	230/280/380	5	30.7782	78.9533	3644	0.929	0.23 ± 0.03	0.06 ± 0.01 (0.01)	0.08 ± 0.01	0.08 ± 0.01	0.08 ± 0.01	0.07 ± 0.01
KAL15	Ice polished surface	m <sub>bd1</sub>	Bedrock	2.5	30.7599	78.9584	3986	0.949	39.50 ± 2.37	8.37 ± 0.50 (0.89)	8.61 ± 1.14	9.08 ± 1.20	8.48 ± 0.98	8.19 ± 0.85
KAL17	Ice polished surface	m <sub>bd1</sub>	Bedrock	2.5	30.7601	78.9585	3974	0.946	42.10 ± 2.95	9.00 ± 0.63 (1.01)	9.24 ± 1.27	9.70 ± 1.33	9.07 ± 1.10	8.84 ± 0.97
KAL18	Moriane ridge	m <sub>bd1</sub>	250/270/360	2	30.7565	78.9629	4132	0.949	0.86 ± 0.12	0.17 ± 0.02 (0.03)	0.21 ± 0.04	0.20 ± 0.04	0.21 ± 0.04	0.19 ± 0.03
KAL19	Moriane ridge	m <sub>bd1</sub>	130/220/340	2	30.7585	78.9627	4182	0.937	1.07 ± 0.08	0.21 ± 0.02 (0.02)	0.25 ± 0.03	0.25 ± 0.03	0.26 ± 0.03	0.24 ± 0.03
KAL20	Moriane ridge	m <sub>bd1</sub>	200/330/410	2	30.7567	78.9628	4115	0.940	3.64 ± 0.30	0.73 ± 0.06 (0.09)	0.83 ± 0.12	0.85 ± 0.12	0.84 ± 0.11	0.80 ± 0.09
KAL21	Moriane ridge	m <sub>bd1</sub>	110/150/240	2	30.7567	78.9653	4108	0.939	0.87 ± 0.12	0.17 ± 0.02 (0.03)	0.21 ± 0.04	0.21 ± 0.04	0.21 ± 0.04	0.20 ± 0.03
KAL23	Ice polished surface	m <sub>bd1</sub>	Bedrock	3	30.7571	78.9628	4093	0.926	38.60 ± 1.93	7.98 ± 0.40 (0.80)	8.19 ± 1.05	8.65 ± 1.11	8.09 ± 0.90	7.80 ± 0.77
KAL24	Ice polished surface	m <sub>bd1</sub>	Bedrock	2	30.7529	78.9733	4498	0.971	53.90 ± 2.16	8.65 ± 0.35 (0.83)	8.65 ± 1.08	9.13 ± 1.14	8.50 ± 0.91	8.47 ± 0.79
<b>Mayali</b>														
KAL25	Moriane ridge	m <sub>m1</sub>	170/200/320	1.5	30.7283	79.0198	4405	0.980	70.00 ± 3.50	11.60 ± 0.58 (1.17)	11.41 ± 1.47	11.87 ± 1.52	11.09 ± 1.23	11.42 ± 1.12
KAL26	Moriane ridge	m <sub>m1</sub>	70/240/250	3	30.7281	79.0198	4412	0.979	66.50 ± 2.66	11.13 ± 0.45 (1.07)	10.98 ± 1.37	11.43 ± 1.42	10.69 ± 1.14	10.96 ± 1.03
KAL27	Moriane ridge	m <sub>m1</sub>	210/310/450	2	30.7280	79.0189	4411	0.972	71.70 ± 0.01	12.00 ± 0.48 (1.15)	11.77 ± 1.47	12.23 ± 1.52	11.42 ± 1.22	11.82 ± 1.11
KAL28	Moriane ridge	m <sub>m1</sub>	210/310/350	3	30.7271	79.0205	4378	0.980	74.40 ± 3.72	12.65 ± 0.63 (1.27)	12.39 ± 1.59	12.84 ± 1.64	12.01 ± 1.33	12.46 ± 1.23
<b>Kedarnath</b>														
KAL40	Active ice	m <sub>k3</sub>	120/150/450	2.5	30.7481	79.0658	3904	1.000	0.25 ± 0.03	0.05 ± 0.01 (0.01)	0.07 ± 0.01	0.07 ± 0.01	0.07 ± 0.01	0.06 ± 0.01
KAL41	Active ice	m <sub>k3</sub>	50/180/220	4	30.7485	79.0642	3892	1.000	0.79 ± 0.31	0.17 ± 0.07 (0.07)	0.21 ± 0.08	0.20 ± 0.08	0.21 ± 0.08	0.19 ± 0.08
KAL42	Active ice	m <sub>k3</sub>	90/80/240	2.5	30.7472	79.0636	3853	1.000	2.19 ± 0.90	0.47 ± 0.19 (0.20)	0.57 ± 0.24	0.57 ± 0.24	0.58 ± 0.24	0.54 ± 0.22
KAL35	Moriane ridge	m <sub>k2</sub>	120/180/250	4	30.7448	79.6503	3841	0.953	1.81 ± 0.41	0.42 ± 0.09 (0.10)	0.51 ± 0.13	0.51 ± 0.13	0.52 ± 0.13	0.48 ± 0.12
KAL36	Moriane ridge	m <sub>k2</sub>	150/250/300	5	30.7454	79.652	3853	0.950	0.80 ± 0.09	0.19 ± 0.02 (0.03)	0.23 ± 0.04	0.22 ± 0.04	0.23 ± 0.03	0.21 ± 0.03
KAL37	Moriane ridge	m <sub>k2</sub>	150/200/220	3	30.7462	79.6555	3884	0.959	72.20 ± 22.20	16.07 ± 4.97 (5.16)	15.72 ± 5.20	16.08 ± 5.32	15.22 ± 4.94	15.65 ± 5.01
KAL38	Moriane ridge	m <sub>k2</sub>	60/130/220	5	30.7473	79.6661	3909	0.959	0.80 ± 0.08	0.18 ± 0.02 (0.02)	0.22 ± 0.03	0.22 ± 0.03	0.22 ± 0.03	0.20 ± 0.03
KAL39	Moriane ridge	m <sub>k2</sub>	150/200/250	2.5	30.7478	79.6662	3915	0.096	1.22 ± 0.22	2.38 ± 0.43 (0.48)	2.66 ± 0.57	2.82 ± 0.61	2.67 ± 0.55	2.54 ± 0.50
KAL29	Moriane ridge	m <sub>k1</sub>	300/400/500	2.5	30.7301	79.0635	3648	0.948	35.70 ± 3.21	9.05 ± 0.82 (1.13)	9.43 ± 1.40	9.87 ± 1.46	9.27 ± 1.24	8.88 ± 1.10
KAL30	Moriane ridge	m <sub>k1</sub>	50/200/250	2.5	30.7296	79.0635	3650	0.948	57.90 ± 9.85	14.68 ± 2.50 (2.81)	14.69 ± 3.05	15.07 ± 3.13	14.25 ± 2.81	14.39 ± 2.74
KAL31	Moriane ridge	m <sub>k1</sub>	100/150/200	2.5	30.7295	79.0635	3642	0.944	36.60 ± 8.06	9.34 ± 2.06 (2.22)	9.72 ± 2.43	10.15 ± 2.54	9.54 ± 2.31	9.19 ± 2.17
KAL32	Moriane ridge	m <sub>k1</sub>	120/150/200	2.5	30.7287	79.0635	3641	0.940	29.60 ± 3.85	7.58 ± 0.99 (1.19)	7.98 ± 1.40	8.42 ± 1.48	7.90 ± 1.29	7.40 ± 1.15
KAL33	Moriane ridge	m <sub>k1</sub>	200/500/600	2	30.7295	79.0635	3643	0.944	32.60 ± 1.63	8.28 ± 0.42 (0.83)	8.66 ± 1.11	9.12 ± 1.17	8.54 ± 0.95	8.09 ± 0.80
KAL34	Moriane ridge	m <sub>k1</sub>	100/150/180	3	30.7244	79.0652	3605	0.958	35.70 ± 1.79	9.20 ± 0.46 (0.92)	9.60 ± 1.23	10.03 ± 1.28	9.43 ± 1.05	9.04 ± 0.89

<sup>a</sup> All samples were gneiss.

<sup>b</sup> Altitudes were determined using a handheld GPS with an uncertainty of ±30 m.

<sup>c</sup> Blanks for KAL1, 2, 3, 9D, 11, 12, 13 samples =  $1.41 \times 10^{-14}$ , KAL4, 5, 7, 14–19, 23–34, 39, 41 and 42 samples =  $1.01 \times 10^{-14}$ , and KAL20, 21, 22D, 35, 36, 37, 38, 40 =  $1.19 \times 10^{-14}$ .

<sup>d</sup> Ages were determined using a rock density of 2.75 g/cm<sup>3</sup> and 07 KNSTD standard. Uncertainties include analytical and production rate/scale model uncertainties.

**Table 2**  
Summary of  $^{10}\text{Be}$  ages for central Garhwal.

Study area	Moraine name	Number of $^{10}\text{Be}$ ages	Range of $^{10}\text{Be}$ ages (ka)	Average and $1\sigma$ $^{10}\text{Be}$ age (ka)	PDF ages and $1\sigma$ (ka)	Likely age	Possible correlation with glacial stages in Bhagirathi Valley, western Garhwal of Sharma and Owen (1996) and Barnard et al. (2004a)
Mayali Pass valley	m <sub>m1</sub>	4	11.0–12.5	11.6 ± 0.6	11.6 ± 0.6	Lateglacial	Bhagirathi glacial stage
Upper Bhillangana and Dudhganga valleys	m <sub>bd4</sub>	2	0.05–0.2	0.1 <sup>a</sup>	0.18 ± 0.09	Recent	
	m <sub>bd3</sub>	5	0.2–2.0	1.6/0.2 <sup>b</sup>	>50% Uncertainty	Little Ice Age	Bhujbas glacial stage
	m <sub>bd2</sub>	5	0.02–0.3	0.3 <sup>c</sup>	>50% Uncertainty	Little Ice Age	Bhujbas glacial stage
	m <sub>bd1</sub>	10	0.2–8.8	8.3 ± 0.4 <sup>d</sup>	8.8 ± 4.2	Early Holocene	Kedar glacial stage
Kedarnath, Upper Mandakini valley	m <sub>k3</sub>	3	0.06–0.5	<sup>e</sup>	>50% Uncertainty	Recent	
	m <sub>k2</sub>	5	0.2–15.7	0.3 ± 0.2 <sup>f</sup>	>50% Uncertainty	Little Ice age	Bhujbas glacial stage
	m <sub>k1</sub>	6	7.4–14.4	8.5 ± 0.8 <sup>g</sup>	9.2 ± 0.6	Early Holocene	Kedar glacial stage

<sup>a</sup> No uncertainty quoted because only a paired sample.

<sup>b</sup> Two pair of ages very similar, no uncertainty quoted because only paired samples.

<sup>c</sup> Excluding all boulder ages KAL3–5, no uncertainty quoted because only paired sample is used.

<sup>d</sup> Excluding boulder ages KAL16, 18–22.

<sup>e</sup> Only three samples so not statistically enough.

<sup>f</sup> Excluding KAL37 and 39, which are probably inherited boulders.

<sup>g</sup> Sample KAL30 is excluded from the average because it is  $\gg 2\sigma$  older than the average of this data set.

numbers to provide a simple naming scheme that can be changed with the addition of new data in the future. Student's *t*-test analysis of  $^{10}\text{Be}$  ages enclosed by selected PDF reveals 27 clearly defined regional glacial stages ( $\geq 98\%$  confidence) and two tentative regional glacial stages (Fig. 10). The chronology plots show that some component PDF ages appear to be closer to a regional stage that is different from the stage indicated by Student's *t*-test. This discrepancy is an artifact of the *t*-test which compares individual  $^{10}\text{Be}$  ages, whereas the plots (Fig. 10) show component PDF ages.

As in Dortch et al. (2013), we use several proxies for precipitation activity in the orogen (Wang et al., 2001, 2008): the Lisiecki and Raymo (2005) stacking of marine  $\delta^{18}\text{O}$  records and NGRIP (2004)  $\delta^{18}\text{O}$  as a proxy for northern hemisphere events and global ice volume; the Leuschner and Sirocko (2003) simulated Indian monsoon index; Thompson et al.'s (1997)  $\delta^{18}\text{O}$  record of the Guliya ice core; and  $\delta^{18}\text{O}$  speleothem East Asian monsoon records (Wang et al., 2001, 2008). The monsoon index peaks correspond to periods of strong monsoons. Dortch et al. (2013) point out that the uncertainty associated with these different proxies is typically  $< 2\%$ , but other proxy chronologies determined through a number of other methods including  $^{14}\text{C}$ ,  $^{36}\text{Cl}$ ,  $^{230}\text{Th}$  chronologies, and orbital tuning can have significantly greater uncertainty.

Of the 205 datasets analyzed using PDF component separation, no age was determined for 28 datasets because they comprise a single age ( $n = 11$ ) or had uncertainties  $\geq 50\%$  ( $n = 17$ ). Another 24 datasets were eliminated due to their component PDF ages being indistinguishable from a previous or subsequent advance (a separate landform), or because the component PDF ages did not follow the morphostratigraphic order laid out in the original publication. Of the ages compiled (1081 + 38 [this study]), a total of 185 ages were eliminated. The remaining 153 datasets (934 remaining ages) were analyzed further using the Student's *t*-test. Of these, 520 ages (56%) were within  $1\sigma$  of component PDF peaks used to define the ages of local glacial stages, 98 ages (10%) were identified as too old, and 316 ages (34%) were identified as too young. Our evaluation of the age data resulted in component PDFs for 102 datasets that define the age of local glacial stages and 51 datasets that define tentative ages for local glacial stages. Graphic representation of all ages compiled here are available in Appendix 3 (in Supplementary items), which contains plots of each local glacial stage arranged in chronological order and grouped into individual files ( $n = 64$ ) based on location.

## 8. Discussion

We first discuss the timing and nature of glaciation in the central Garhwal as inferred from our new  $^{10}\text{Be}$  ages. Then, on the basis of our new results, we discuss regional glaciation throughout the monsoon-influenced Himalayan–Tibetan orogen. We conclude with a discussion of the climatic significance of the MOHITS.

### 8.1. Central Garhwal

Our mapping and dating of moraines in central Garhwal shows that glaciation was restricted in its extent during the Lateglacial through the Holocene. We see no evidence for glaciation earlier than the Lateglacial. It seems likely that there were glacial stages in this area before this time, so the absence of glacial landforms indicates that either erosion destroyed older landforms or that the Lateglacial Advance was more extensive than earlier advances and removed the older glacial features. Our data do not address the lack of older glacial landforms, but some combination of erosion and later glacial advance must be responsible.

The impressive Lateglacial and Early Holocene moraines in central Garhwal are also common in other areas of the monsoon-influenced Himalaya (Owen, 2009 and references therein); these moraines might be interpreted as glacial advances during the Younger Dryas Stadial and the 8.2 ka cooling event, respectively. We are cautious about assigning such ages because the uncertainty associated with TCN production rates makes such correlations tentative. Owen et al. (2001) hypothesized that similar age advances in the Lahul Himalaya were related to a greater influence of the monsoon on positive glacier mass balances during the Lateglacial Interstadial and Early Holocene. This may well be the case in central Garhwal as well.

The Late Holocene advances in central Garhwal are restricted (generally  $< 1$  km) in extent and likely represent Neoglaciation and possibly LIA advances. This contrasts with many other parts of the world where Neoglaciation advances were the most extensive during the Holocene (Grove, 2004).

Comparison of the central Garhwal glacial record and that for the upper Bhagirathi valley in western Garhwal to the north is striking (Table 2). Like the upper Bhagirathi valley, there is an Early Holocene advance, the Kedar glacial stage of Sharma and Owen (1996) and Barnard et al. (2004a), and an LIA advance, the



**Table 3**

Details of local and regional glacial stages including name, age, *p*-values, and suggested climate correlations using the methods of [Dortch et al. \(2013\)](#). Column four represents the range of *p*-values when testing clusters of <sup>10</sup>Be ages between local glacial stages. All *p*-values are greater than 0.05 which suggests there is no reason to reject the null hypothesis and that the local glacial stages may belong to a single normal distribution. Column six contains *p*-values for the comparison of combined regional glacial stage <sup>10</sup>Be age sets. Here, *p*-values less than 0.05 indicates that the regional <sup>10</sup>Be age sets are distinct and separate at >95% confidence level. Note: the name and age of tentative local glacial stages are shown in italics.

Regional glacial stage	Local Glacial stage	Local stage age (ka)	P-values between local glacial stages	Regional stage age (ka)	P-values between local glacial stages	Climate correlation
MOHITS 13 [tentative]	M1c of Owen et al. (2010)	516 ± 64	N/A	483 ± 38	0.01	MIS 13, unknown
	<i>T1 of Owen et al. (2009)</i>	360 ± 33				
MOHITS 9	4c, M3old of Chevalier et al. (2011)	304 ± 140	0.41–0.67	314 ± 48	0.00	MIS 8–10, unknown
	M2E of Chevalier et al. (2005)	301 ± 48				
MOHITS 7	<i>Nata, outermost sequence (sample group Q) of Fu et al. (2013)</i>	211 ± 44	0.58–0.93	192 ± 10	0.00	MIS 6/7, Monsoon
	<i>Nyalam moraine sequence: Moraine #3 of Schaefer et al. (2008)</i>	210 ± 28				
	<i>Tanggula glacial stage of Schäfer et al. (2002)</i>	190 ± 27				
MOHITS 6B	17a, CK M3 of Chevalier et al. (2011)	178 ± 27	0.96	168 ± 12	0.00	MIS 6, Monsoon
	Kuzhaori valley of the Haizishan Plateau, outermost sequence (sample group A) of Fu et al. (2013)	175 ± 23				
MOHITS 6A	M2W (oldest moraine, west) of Chevalier et al. (2005)	154 ± 15	0.21–0.98	143 ± 12	0.00	MIS 6, Monsoon & mid-latitude westerlies
	Xinlong Plateau, outermost sequence (sample group O) of Fu et al. (2013)	152 ± 6				
	J, BH-3 of Heyman et al. (2011)	150 ± 40				
	Area C, Guxiang Glaciation of Zhou et al. (2007, 2010)	143 ± 14				
MOHITS 5E [tentative]	8, Dingye N of Chevalier et al. (2011)	140 ± 40	N/A	121 ± 5	0.00	MIS 5e, Monsoon
	Bashico glacial stage of Owen et al. (2005)	122 ± 15				
MOHITS 5B	M1 moraine of Mériaux et al. (2004)	106 ± 16	0.43–0.95	91 ± 15	0.00	MIS 5b, mid-latitude westerlies
	<i>I, ? of Heyman et al. (2011)</i>	104 ± 35				
	M1 moraines of Owen et al. (2006b)	98 ± 24				
	12B, Pulan M2 of Chevalier et al. (2011)	96 ± 24				
	Thyangboche I glacial stage of Finkel et al. (2003)	95 ± 35				
MOHITS 4	G: BH-2 of Heyman et al. (2011)	90 ± 19	0.32–0.78	68 ± 10	0.00	MIS 4, mid-latitude westerlies
	<i>Naisa valley moraines: older ridge of Schaefer et al. (2008)</i>	80 ± 37				
MOHITS 3C	M2 of Owen et al. (2010)	78 ± 11	0.37–0.91	55 ± 5	0.00	MIS 3, monsoon
	17c, CK M2 outer of Chevalier et al. (2011)	76 ± 18				
	M2 moraine of Mériaux et al. (2004)	73 ± 14				
	M3 of Owen et al. (2010)	66 ± 18				
	<i>No stage name given of Kong et al. (2009b)</i>	60 ± 4				
	M4 of Owen et al. (2010)	60 ± 11				
	M4a of Owen et al. (2010)	60 ± 17				
	M4a of Owen et al. (2010)	60 ± 2				
	Un-named (oldest) moraine of Owen et al. (2005)	59 ± 6				
	MK2, LGM of Abramowski (2004)	58 ± 12				
2c, ybj outer E of Chevalier et al. (2011)	58 ± 7					
MOHITS 3B	<i>Anyemaqen glacial stage of Owen et al. (2003a)</i>	55 ± 6	0.48–0.93	46 ± 5	0.01	MIS 3, monsoon
	14, WXS of Chevalier et al. (2011)	55 ± 6				
	D, BH-1 of Heyman et al. (2011)	54 ± 18				
	3a, M4 #1 of Chevalier et al. (2011)	54 ± 26				
	5, M2 of Chevalier et al. (2011)	51 ± 9				
MOHITS 3A	12c, Pulan M1E of Chevalier et al. (2011)	51 ± 12	0.565–0.56	42 ± 2	0.00	MIS3, monsoon
	M4b of Owen et al. (2010)	50 ± 4				
	No stage name given of Kong et al. (2009b)	48 ± 14				
	Qitai Valley, Group A moraines of Wang et al. (2013)	47 ± 6				
MOHITS 3A	<i>Jiukehe glacial stage of Owen et al. (2003a)</i>	46 ± 15	0.565–0.56	42 ± 2	0.00	MIS3, monsoon
	<i>Thyangboche II glacial stage of Finkel et al. (2003)</i>	43 ± 4				
	4a, M3 main of Chevalier et al. (2011)	43 ± 2				
	M1 moraine of Chevalier et al. (2005)	42 ± 4				

(continued on next page)

Table 3 (continued)

Regional glacial stage	Local glacial stage	Local stage age (ka)	P-values between local glacial stages	Regional stage age (ka)	P-values between local glacial stages	Climate correlation
MOHITS 2G	<i>Longistai glacial stage (youngest) of Colgan et al. (2006)</i>	38 ± 13				
	2a, ybj outer W of Chevalier et al. (2011)	37 ± 7				
	T2 of Owen et al. (2009)	31 ± 2	0.13–0.77	31 ± 3		MIS 3, H3, monsoon
	6, M1 of Chevalier et al. (2011)	30 ± 1				
	10, Cho Oyo of Chevalier et al. (2011)	30 ± 0.1				0.00
MOHITS 2F	T3 of Owen et al. (2009)	28 ± 3				
	<i>Nar Glacier and (LGM) of Pratt-Sitaula (2004)</i>	27 ± 9				
	<i>Fu Qu valley, Pultuo moraine sequence; Pultuo I moraine of Schaefer et al. (2008)</i>	27 ± 7	0.58–0.84	26 ± 2		MIS 3, monsoon
	MK5: Late Glacial of Abramowski (2004)	27 ± 8				0.00
	2d, ybj outer N of Chevalier et al. (2011)	25 ± 9				
MOHITS 2E	Periche I glacial stage of Finkel et al. (2003)	24 ± 3				
	Qitai Valley, Group B moraines of Wang et al. (2013)	24 ± 2				
	12a, Pitan MHW of Chevalier et al. (2011)	24 ± 2				
	9a, Dingye S frontal of Chevalier et al. (2011)	23 ± 2	0.35–0.98	22 ± 2		MIS 2, H2, mid-latitude westerlies
	t1 moraine of Owen et al. (2003b)	23 ± 6				
	<i>Northern part of Haizhishan Plateau, intermediate sequence (sample group N) of Fu et al. (2013)</i>	22 ± 2				
	<i>Cuo Ji Gang Wa and Cuo Naleng paleoglaciators: outer end moraine of Graf et al. (2008)</i>	22 ± 0.5				
	<i>Pin Valley, Lateral moraine (no stage name) of Scherler et al. (2010)</i>	21 ± 0.3				
	Ximenetuo glacial stage of Owen et al. (2003a)	21 ± 3				0.00
	<i>Cuo Ji Gang Wa and Cuo Naleng paleoglaciators: middle end moraine of Graf et al. (2008)</i>	20 ± 1				
MOHITS 2D	Lateral moraine, Glacier Observation Station of Kong et al. (2009a)	20 ± 4				
	Un-named (intermediate age) moraine of Owen et al. (2005)	19.9 ± 1.4	0.28–0.92	18.7 ± 1.8		MIS 2, OD, monsoon & mid-latitude westerlies
	11, KungCo of Chevalier et al. (2011)	19.3 ± 7.7				
	<i>Cuo Ji Gang Wa and Cuo Naleng paleoglaciators: inner end moraine of Graf et al. (2008)</i>	18.4 ± 1.2				
	1b, Gulu E of Chevalier et al. (2011)	18.0 ± 0.7				0.01
MOHITS 2C	LGM moraine (Laolongwan valley) of Owen et al. (2003c)	17.8 ± 1.3				
	Un-named moraine (oldest) of Schäfer et al. (2002)	17.5 ± 0.5				
	Qitai Valley, Group C moraines of Wang et al. (2013)	17.4 ± 0.2				
	12, EXS of Chevalier et al. (2011)	17.3 ± 1.4	0.44–0.67	17.3 ± 0.5		MIS 2, OD, monsoon & mid-latitude westerlies
	T3' of Owen et al. (2009)	17.1 ± 0.4				
	T2 of Owen et al. (2003b)	17.1 ± 4.5				
	9b, Dingye S main #1 of Chevalier et al. (2011)	17.1 ± 3.6				0.00
MOHITS 2B	West younger moraine: Baiyu Glaciation of Zhou et al. (2007, 2010)	16.9 ± 0.9				
	M4b of Owen et al. (2010)	16.7 ± 0.1				
	Qiemuqu glacial stage of Owen et al. (2003a)	16.6 ± 4.5				
	L12 of Abramowski (2004)	16.5 ± 0.8				
	<i>Pangri Glacier (LGM) of Pratt-Sitaula (2004)</i>	16.3 ± 7.3				
	1a, Gulu W of Chevalier et al. (2011)	16.2 ± 1.0				
	<i>Un-named (oldest) moraine of Owen et al. (2005)</i>	16.0 ± 1.0				
	Chuanxi and northern outlet glacier of Graf et al. (2008)	16.0 ± 2.8				
	<i>Naisa valley moraines, younger ridge of Schaefer et al. (2008)</i>	15.8 ± 1.6				
	Haizhishan Plateau surface, innermost sequence (sample group J) of Fu et al. (2013)	15.7 ± 2.9	0.29–0.97	15.5 ± 1.3		MIS 2, OD, mid-latitude westerlies
Periche II glacial stage of Finkel et al. (2003)	15.6 ± 1.3					
7, M of Chevalier et al. (2011)	15.4 ± 5.0					
Batal glacial stage of Owen et al. (2001)	15.3 ± 1.6				0.00	

Regional glacial stage	Local Glacial stage	Local stage age (ka)	P-values between local glacial stages	Regional stage age (ka)	P-values between local glacial stages	Climate correlation
MOHITS 2B (cont'd)	<i>East moraines: Baiyun Glaciation of Zhou et al. (2007, 2010)</i>	14.9 ± 2.1				
	T4 of Owen et al. (2009)	14.9 ± 1.4				
	<i>Tons Valley (location B): Ganggar lateral moraine (no stage name) of Scherler et al. (2010)</i>	14.9 ± 0.5	0.29–0.97	15.5 ± 1.3	0.00	MIS 2, OD, mid-latitude westerlies
	Zheduo valley moraine ridge of Strasky et al. (2009)	14.9 ± 0.5				
	<i>Un-named (younger) moraine of Owen et al. (2005)</i>	14.7 ± 0.9				
MOHITS 2A	Khudi Glacier (Younger Dryas) of Pratt-Sitaula (2004)	14.1 ± 0.5			0.00	
	LGM moraine (Gangshiga valley) of Owen et al. (2003c)	13.9 ± 1.5				
	M5 of Owen et al. (2010)	13.6 ± 1.0				
	Kicho Glacier (Younger Dryas) of Pratt-Sitaula (2011)	13.6 ± 0.6				
	M2' moraines of Owen et al. (2006b)	13.5 ± 3.1	0.16–0.90	12.9 ± 0.9		MIS 2, H0, Alleröd, Monsoon
	Nar main (Late Glacial) of Pratt-Sitaula (2004)	13.3 ± 1.5				
	MK7, Neoglacial of Abramowski (2004)	13.3 ± 0.8				
	Midim Glacier (Younger Dryas) of Pratt-Sitaula (2011)	13.1 ± 0.3				
	4b, M3 inner of Chevalier et al. (2011)	12.5 ± 1.4				
	2b, ybj inner of Chevalier et al. (2011)	12.5 ± 3.1				
MOHITS 1K	Kulti glacial stage of Owen et al. (2001)	12.4 ± 1.2			0.00	
	<i>Tons Valley (location C) of Scherler et al. (2010)</i>	12.3 ± 0.1				
	Halong glacial stage of Owen et al. (2003a)	12.0 ± 2.7				
	<i>Qitai Valley, Group D moraines of Wang et al. (2013)</i>	11.8 ± 0.3				
	<i>No stage name given of Kong et al. (2009b)</i>	11.6 ± 0.8	0.16–0.85	11.4 ± 0.7		MIS 1, YD, mid-latitude westerlies
	m <sub>1</sub> of Murari et al. (in prep)	11.6 ± 0.6				
	Fu Qu valley, Puluo moraine sequence: Puluo 2 moraine of Schaefer et al. (2008)	11.6 ± 0.5				
	unnamed moraine of Lasserre et al. (2002)	11.5 ± 3.3				
	Lysapche Glacier (early Holocene) of Pratt-Sitaula (2004)	10.6 ± 1.0				0.00
	<i>Un-named (intermediate age) moraine of Owen et al. (2005)</i>	10.6 ± 0.6				
MOHITS 1J	<i>Un-named (intermediate age) moraine of Owen et al. (2005)</i>	10.6 ± 0.6	0.43–0.96	10.1 ± 0.5		MIS 1, 10.3 event, mid-latitude westerlies
	<i>Yak Glacier (lower Younger Dryas) of Pratt-Sitaula (2004)</i>	10.1 ± 2.3				
	Chhukung glacial stage of Finkel et al. (2003)	10.0 ± 0.4				
	L13, Langtang Stage of Abramowski (2004)	9.4 ± 0.7				0.00
	m <sub>basal</sub> of Murari et al. (this paper)	9.2 ± 0.6	0.35–0.58	9.1 ± 0.3		MIS 1, 9.3 event, mid-latitude westerlies
MOHITS 1H	m <sub>basal</sub> of Murari et al. (this paper)	8.8 ± 4.2			0.02	
	<i>Tons Valley (location F') of Scherler et al. (2010)</i>	8.7 ± 0.5				
	<i>Holocene moraine (Gangshiga valley) of Owen et al. (2003c)</i>	8.6 ± 3.3	0.44–0.65	8.1 ± 0.8		MIS 1; 8.2 event, mid-latitude westerlies
	Local LGM moraines of Owen et al. (2005)	8.3 ± 0.5				
	Syakran Glacier (early-mid Holocene) of Pratt-Sitaula (2011)	7.9 ± 0.4				0.00
MOHITS 1G	Danfö Glacier (early-mid Holocene) of Pratt-Sitaula (2004)	7.8 ± 0.3				
	Yak upper (early-mid Holocene) of Pratt-Sitaula (2004)	7.6 ± 0.3				
	M2 moraines of Owen et al. (2006b)	7.1 ± 1.3	0.12–0.82	7.7 ± 0.6		MIS1, 7.4 event?, mid-latitude westerlies
	Kedar glacial stage of Barnard et al. (2004a)	7.0 ± 0.5				
	M3 of Gayer et al. (2006)	6.3 ± 0.6				0.00
MOHITS 1F	<i>"Recessional moraine" of Owen et al. (2005)</i>	6.3 ± 1.8	0.45–0.78	5.4 ± 0.6		MIS 1; Climatic optimum, monsoon
	<i>Tons Valley (location E) of Scherler et al. (2010)</i>	5.4 ± 0.5				
	Langtang glacial stage of Barnard et al. (2006)	4.3 ± 1.3				0.00
	M8 of Owen et al. (2010)	4.3 ± 0.8				
	Moraine m2 of Barnard et al. (2004b)	3.7 ± 1.3				
MOHITS 1E	MK4, L1A of Abramowski (2004)	3.6 ± 0.6	0.12–0.75	3.5 ± 0.4		MIS 1; Neoglacial, monsoon
	<i>Thakha glacial stage of Finkel et al. (2003)</i>	3.5 ± 0.3				
	L16 of Abramowski (2004)	3.4 ± 0.2				0.00

(continued on next page)

Table 3 (continued)

Regional glacial stage	Local Glacial stage	Local stage age (ka)	P-values between local glacial stages	Regional stage age (ka)	P-values between local glacial stages	Climate correlation
MOHITS 1D	T5c of Owen et al. (2009) <i>Un-named (youngest) moraine of Owen et al. (2005)</i>	2.4 ± 0.4 2.2 ± 0.3	0.31	2.3 ± 0.1	0.00	MIS 1; Neoglacial, monsoon
MOHITS 1C	Neoglacial of Zech et al. (2009) T6 of Owen et al. (2009)	1.6 ± 0.4 1.6 ± 0.1	0.56	1.5 ± 0.2	0.00	MIS 1; Neoglacial, mid-latitude westerlies
MOHITS 1B	Neoglacial moraines of Owen et al. (2005) <i>Gangotri glacial stage of Barnard et al. (2004a)</i> <i>Tons Valley (location G) of Scherler et al. (2010)</i>	0.9 ± 0.2 0.8 ± 0.3 0.7 ± 0.3	0.35–0.45	0.7 ± 0.1	0.00	MIS 1; Neoglacial, mid-latitude westerlies
MOHITS 1A	<i>Moraine m4 of Barnard et al. (2004b)</i> Yala 1 glacial stage of Barnard et al. (2006) <i>W moraine crest of Heimsath and McGlynn (2008)</i> E moraine crest of Heimsath and McGlynn (2008) M9 of Owen et al. (2010) T7 of Owen et al. (2009) <i>Little Ice Age moraines of Owen et al. (2005)</i>	0.6 ± 0.2 0.6 ± 0.1 0.5 ± 0.3 0.5 ± 0.2 0.4 ± 0.1 0.4 ± 0.1 0.4 ± 0.1	0.13–0.93	0.4 ± 0.1		MIS 1; Little Ice Age, mid-latitude westerlies

### 8.2.1. Pre-Last Glacial cycle

We grouped 15 local glacial stages >110 ka in age into 6 regional stages. Two of these (MOHITS 13 at  $483 \pm 38$  ka and 5E at  $121 \pm 5$  ka) are tentative as they only represent one local glacial stage. However, we include them because their ages are unique and distinguish them from other local and regional glacial stages at a confidence level greater than 99%.

MOHITS 13 at  $483 \pm 38$  ka yields a reasonable MAD of  $\sim 8\%$ , but the uncertainty is too large to compare it with MIS stages and the simulated monsoon index of Lisiecki and Raymo (2005) and Leuschner and Sirocko (2003), respectively (Fig. 10B). Evidently, old terrestrial glacial landforms can be preserved in more arid (<500 mm/yr precipitation) monsoon-influenced regions.

MOHITS 9 occurs in three separate areas that have a mean and MAD of  $314 \pm 48$  ka. The large scatter of ages within the local glacial stages leads to the large MAD uncertainty. Thus, we cannot be more precise than potential correlation with MIS 8–10 and monsoon peaks 14–17.

MOHITS 7 ( $192 \pm 10$  ka), MOHITS 6B ( $168 \pm 12$  ka), MOHITS 6A ( $143 \pm 12$  ka), and MOHITS 5E ( $121 \pm 5$  ka) each contain 1–5 local glacial stages which are typically (10 of 11) from arid regions with <500 mm/yr precipitation (Fig. 11). The smaller MAD uncertainties ( $\leq 8\%$ ) of these regional stages enable their tentative correlation to monsoon peaks 6–9 and MIS stages 5E, 6, and 7. The contemporary arid position and alignment of these regional stages with the trailing edge of monsoon peaks is striking and suggests that the glaciers retreated primarily in response to reduced monsoonal moisture supplies. In contrast, MOHITS 6A has the largest spatial representation and overlaps with the coldest portion of MIS 6; thus, there may be a mixed climate signal regionally with some glaciers responding to cold and decreased melting, while others respond strongly to monsoon precipitation.

No significant spatial pattern of the locations of regional glacial stages >110 ka is observable except that most (14 of 15) occur in high mountain and plateau areas and the large majority of local sites have a contemporary semi-arid setting. Arid environments help preserve older landforms and allows them to be dated. Future dating of older landforms in dry regions will likely reduce uncertainties associated with MOHITS 5E, 9, and 13.

### 8.2.2. The Last Glacial cycle

We grouped 91 local glacial stages, ranging in age from 12.5 ka to 106 ka, into 12 regional stages (Fig. 12; ~). The number of local glacial stages within each regional stage varies from 3 to 19. They are discussed in chronological order below.

MOHITS 5B ( $91 \pm 15$  ka) and MOHITS 4 ( $68 \pm 10$  ka) contain six and five local glacial stages, respectively. The majority of these local stages (8 of 11) occur in drier areas with <500 mm/yr precipitation. In contrast to the previous group, these two regional stages occur centrally in monsoon troughs and correlate extremely well with negative  $\delta^{18}\text{O}$  excursions from the Guliya ice core of Thompson et al. (1997) and the cold trough of MIS 4 and 5B. These correlations suggest that cold and precipitation brought by the mid-latitude westerlies led to increased accumulation which forced glaciation; the subsequent rise in temperature and monsoon strength weakened the mid-latitude westerlies and triggered glacial retreat.

MOHITS 3C ( $55 \pm 5$  ka), MOHITS 3B ( $46 \pm 5$  ka), and MOHITS 3A ( $42 \pm 2$  ka) contain eleven, six, and three local glacial stages, respectively. In a similar pattern, the majority (14 of 17) occurs in arid areas with <500 mm/yr precipitation. MOHITS 3C, 3B, and 3A cluster chronologically in early, mid, and late MIS 3, respectively, but with distinct gaps separating them from stages in MIS 2 and 4. The mean of these regional stages do align within 100 years of pronounced negative  $\delta^{18}\text{O}$  excursions from the Guliya ice core

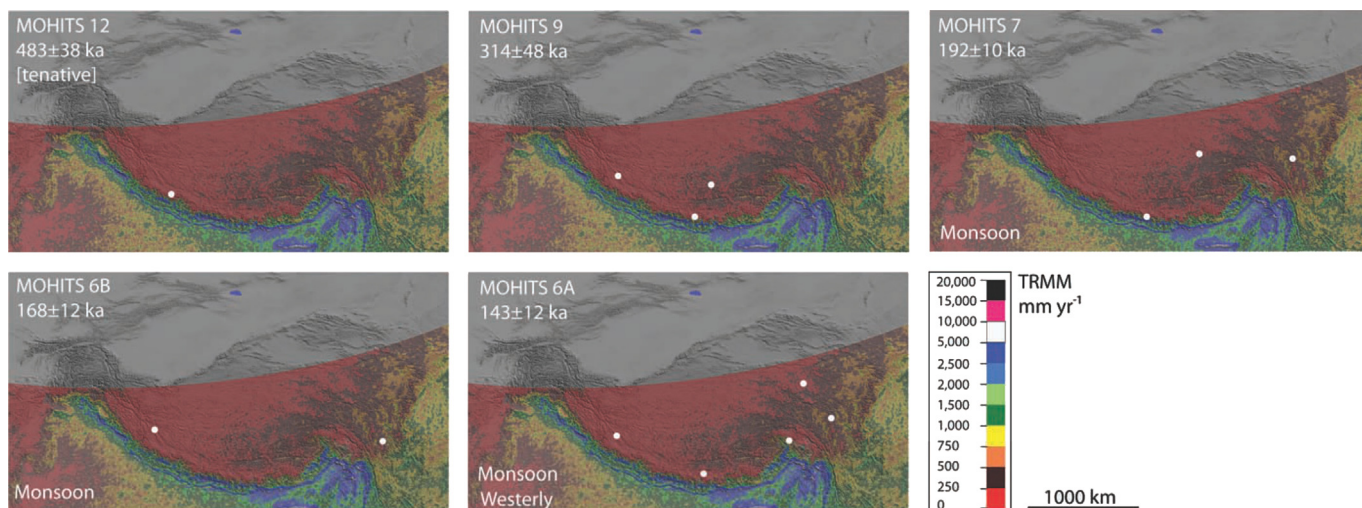


**Fig. 11.** SRTM hillshade images of the study area draped with semi-transparent TRMM imagery from 1998 to 2008 (Bookhagen and Burbank, 2006, 2010; <http://www.geog.ucsb.edu/~bodo/TRMM/>) for pre-Last Glacial cycle regional glacial stages (MOHITS 13–6A). Local glacial stage locations are marked by white dots and the suggested climatic driver (Monsoon – south Asian summer monsoon; Westerly – mid-latitude westerlies) is labeled in bottom left corner of each panel.

(Thompson et al., 1997). Moreover, MOHITS 3A, 3B, and 3C occur on or after monsoon peak 3, which suggests that decreasing monsoon precipitation lead to deglaciation. Confirmation of this would come from interior plateau regions undergoing deglaciation, first followed by Greater Himalaya marginal sites that receive significantly more precipitation. Unfortunately, this is only suggested between MOHITS 3C to 3B by a weak regional spatial pattern that then seems to reverse in MOHITS 3A. The weak spatial pattern may be consequence of local topographic controls over glaciation and deglaciation, or it could be an artifact caused by the reduced number of sediments dated to MOHITS 3B and 3A.

MOHITS 2G and 2F contain five and four local glacial stages, respectively. While all MOHITS 2G sites are in areas where there is <500 mm/yr precipitation, MOHITS 2F sites are in wetter areas near the margin of the plateau. MOHITS 2G mean and MAD of  $31 \pm 3$  ka occurs during declining  $65^\circ\text{N}$  insolation and the end of the monsoon index plateau. There is a sharp negative  $\delta^{18}\text{O}$  excursion shown in the Guliya ice core and increasing cold toward MIS 2 at this time. MOHITS 2G at  $\sim 31$  ka is most likely due to the decreasing strength of the monsoon providing less precipitation, leading to glacier starvation and retreat. MOHITS 2F has an age of  $26 \pm 2$  ka and appears to have responded to similar forcing, but glaciers in this stage seem to have been able to maintain their position or re-advance. This correlates with a positive  $\delta^{18}\text{O}$  excursion in the Guliya ice core and with decreasing precipitation toward the trough between monsoon index peaks 1 and 2. The climatic correlations and spatial patterns of MOHITS 2G suggest that monsoon precipitation penetrated beyond the Himalaya deep into the arid Tibetan plateau. Cool sea surface temperatures associated with Heinrich event 3 likely caused the cessation of the MOHITS 2G stage. Some glaciers were likely sustained by their proximity to the edge of the Himalayan–Tibetan orogen, for example those of MOHITS 2F where the weakening monsoon could still deliver enough moisture to accumulation areas until the conditions leading up to MIS-2 became too unfavorable.

MOHITS 2E comprises nine local glacial stages and has widespread spatial distribution except for the interior of the Tibetan plateau. The majority (7 of 9) of areas with dated local glacial stages receive <500 mm/yr of contemporary precipitation. Chronologically, this regional stage has an age of  $22 \pm 2$  ka and occurs out of synchronization with the Guliya ice core record during a positive  $\delta^{18}\text{O}$  excursion and also in the middle of a weak monsoon index

trough. It is correlated with MIS-2 and the gLGM as defined by Mix et al. (2001) at  $21 \pm 2$  ka and ends immediately after Heinrich event 2. Even though temperatures decrease toward the MIS-2  $\delta^{18}\text{O}$  maximum, the increasing monsoon and weakening of the mid-latitude westerlies likely terminated this glacial stage.

The mean and MAD of regional glacial stages that are younger than the gLGM as defined by Mix et al. (2001) are not altered significantly by using various geomagnetic corrections (Dortch et al., 2013). Accordingly, for the remaining regional glacial stages discussed below, climatic correlations are more robust.

MOHITS 2D ( $18.7 \pm 1.8$  ka;  $n = 7$ ), MOHITS 2C ( $17.3 \pm 0.5$  ka;  $n = 6$ ), and MOHITS 2B ( $15.5 \pm 1.3$  ka;  $n = 19$ ) each comprise several local glacial stages, most of which (25 of 32) occur in regions with <500 mm/yr of contemporary precipitation, and occur within the timeframe of the Oldest Dryas. Local glacial stages from MOHITS 2D and 2C occur on the eastern and southern portions of the Tibetan plateau, respectively, while MOHITS 2B has excellent spatial representation across the plateau excluding its interior.

MOHITS 2D is in phase with the Guliya ice core and speleothem negative  $\delta^{18}\text{O}$  excursion and the low  $\delta^{18}\text{O}$  trough present throughout MIS-2. This suggests that strong monsoons and cool temperatures were responsible for bringing moisture deep into the Tibetan plateau interior and staving off some summer melting, respectively. MOHITS 2C occurs at the end of this trend where both the Guliya ice core and speleothem  $\delta^{18}\text{O}$  records are moving towards a positive excursion, signaling the weakening of the monsoon. Monsoon weakening is also indicated by the start of Heinrich event 1 immediately after MOHITS 2C. We suggest that the increase in temperature and a decrease in precipitation triggered deglaciation. Thus, MOHITS 2D and 2C were likely part of the same advance with glaciers more sensitive to temperature terminating their advance in MOHITS 2D and those more sensitive to precipitation terminating their advance in MOHITS 2C. Furthermore, we suggest that both of these stages were primarily driven by the monsoon and that the lack of a distinct spatial pattern to either one is due to a paucity of locations sampled over the >2000 km wide region as well as local factors affecting the sensitivity of glaciers to temperature and precipitation.

In contrast, MOHITS 2B culminates just after a deep negative trough in the NGRIP and speleothem  $\delta^{18}\text{O}$  records and a smaller negative excursion for the Guliya ice core. This timing suggests that the northern hemisphere cold event was promoting ice

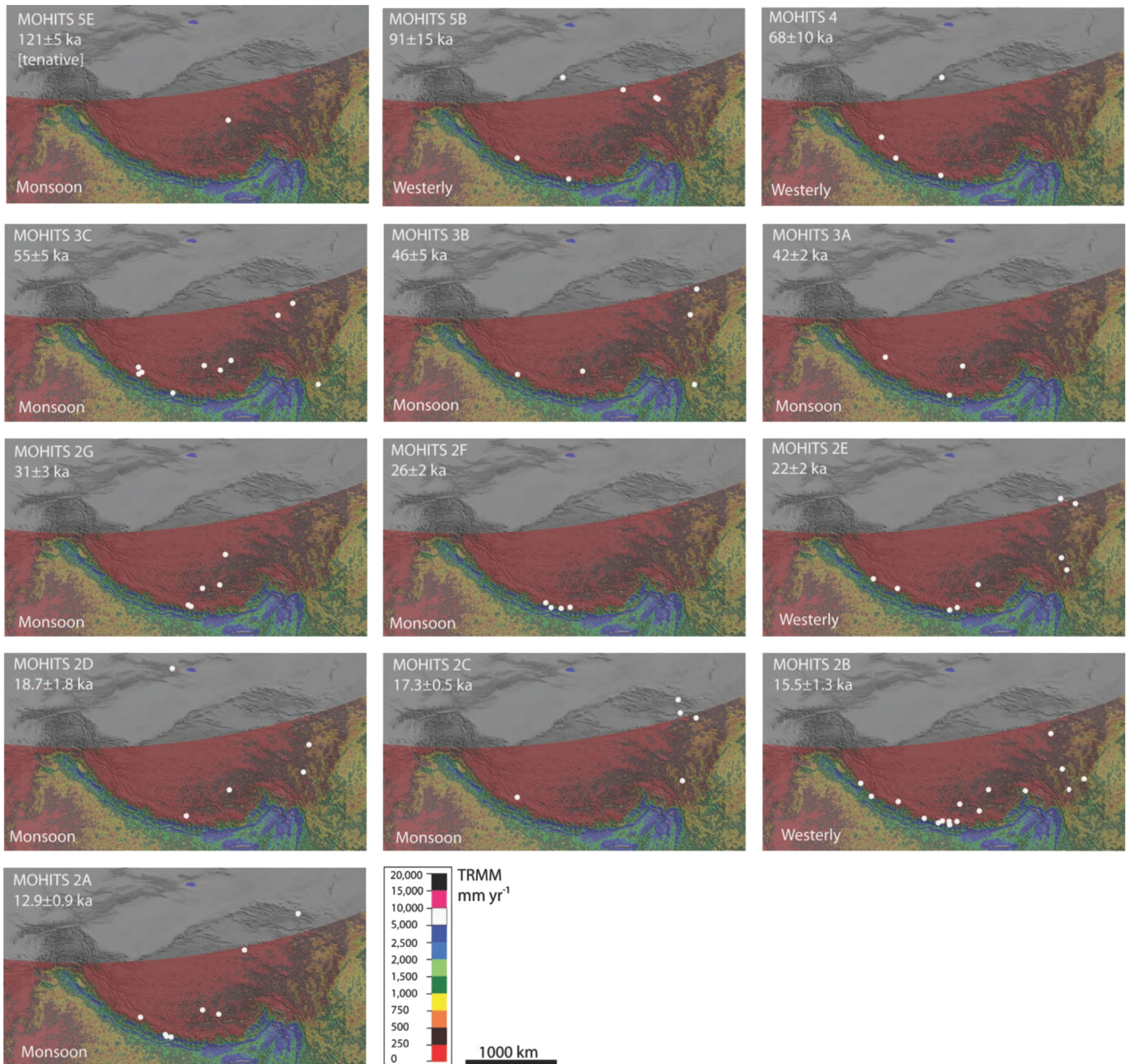


**Fig. 12.** SRTM hillshade images of the study area draped with semi-transparent TRMM imagery from 1998 to 2008 (Bookhagen and Burbank, 2006, 2010; <http://www.geog.ucsb.edu/~bodo/TRMM/>) for the Last Glacial–Interglacial cycle regional glacial stages (MOHITS 5E–2A). Local glacial stage locations are marked by white dots and the suggested climatic driver (Monsoon – south Asian summer monsoon; Westerly – mid-latitude westerlies) is labeled in bottom left corner of each panel.

accumulation on the Tibetan plateau through the reduction of summer melting. MOHITS 2B occurs just after the cold events in all three proxy records; the increase in monsoon strength, indicated by the subsequent positive speleothem  $\delta^{18}\text{O}$  excursion, terminated this regional glacial stage. This is significant because MOHITS 2B is the most represented glacial stage ( $n = 19$ ) across the monsoon influenced Himalaya–Tibetan orogen and it was most likely driven by the mid-latitude westerlies.

MOHITS 2A is comprised of ten local glacial stages and has a mean and MAD of  $12.9 \pm 0.9$  ka. The SW–NE oriented spatial distribution of the local glacial stages that changes across the plateau is likely the result of the distribution of studies. There is an even split between local stages in wet and arid areas. The timing of this

regional glacial stage occurs after a positive excursion in the NGRIP and Guliya  $\delta^{18}\text{O}$  records and a negative speleothem  $\delta^{18}\text{O}$  excursion. Stage termination is out of phase with the Guliya ice core record, which shows increased accumulation at this time. MOHITS 2A also correlates with the end of the Allerød; thus, we suggest that this stage was driven by monsoon precipitation and that the decreasing strength of the monsoon as shown by the speleothem records led to deglaciation.

### 8.2.3. The Holocene

There are 47 local glacial stages that range from 0.4 to 12.4 ka in age that can be grouped into 11 regional stages (Fig. 13, Table 3). The number of local glacial stages within each regional stage varies

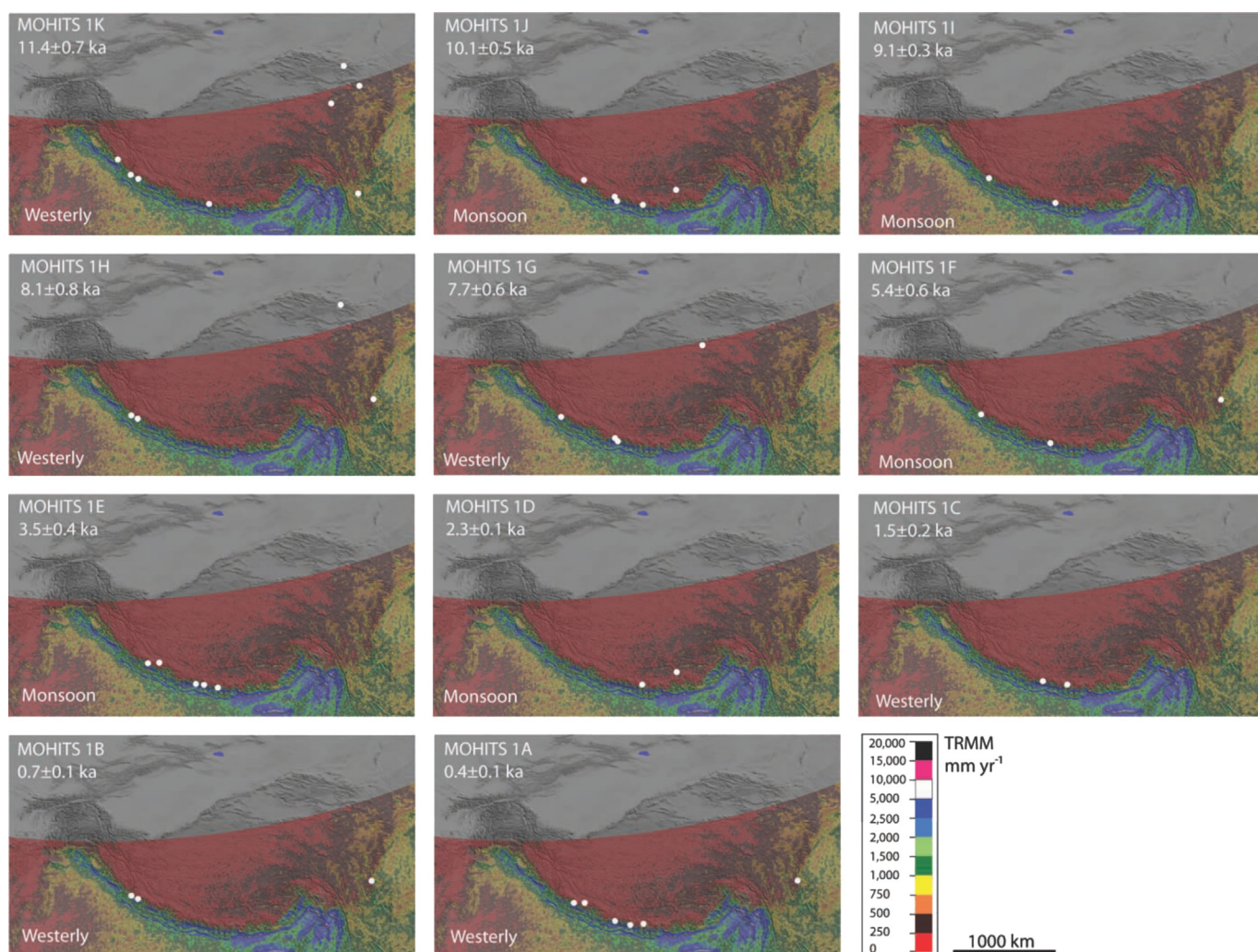


**Fig. 13.** SRTM hillshade images of the study area draped with semi-transparent TRMM imagery from 1998 to 2008 (Bookhagen and Burbank, 2006, 2010; <http://www.geog.ucsb.edu/~bodo/TRMM/>) for MOHITS 1K–1A. Local glacial stage locations are marked by white dots and the suggested climatic driver (Monsoon – south Asian summer monsoon; Westerly – mid-latitude westerlies) is labeled in the bottom left corner of each panel.

from 2 to 8. Generally, the smaller uncertainties enable better correlation with climatic events even though the percentage error becomes larger ( $\sim 25\%$ ) for regional stages with ages less than 1 ka. Regional glacial stages are discussed in chronological order below.

MOHITS 1K ( $11.4 \pm 0.7$  ka) is a very early Holocene event that has the largest representation ( $n = 8$ ) of all recent periods of advance. The majority of local glacial stages (5 of 8) occur in wetter regions with  $>1000$  mm/yr of contemporary precipitation. Our  $m_{m1}$  in the Mayali Pass valley study area belongs to MOHITS 1K. The spatial distribution of the local glacial stages is limited to the southern and eastern edges of the Tibetan plateau. Chronologically, this stage terminates immediately after the Younger Dryas as represented by the NGRIP  $\delta^{18}\text{O}$  record while the speleothem  $\delta^{18}\text{O}$  records shows that the monsoon is gaining intensity and the Guliya ice core shows decreased accumulation. Even though the age of this regional glacial stage is within the Holocene, we suggest that it represents deglaciation after the Younger Dryas cold event. Our interpretation highlights the fact that deglaciation ages represent the end of a glacial advance and the initial stabilization of glacial landforms; they do not give any indication about the duration of the glacial advance that they represent.

MOHITS 1J ( $10.1 \pm 0.5$  ka;  $n = 5$ ), MOHITS 1I ( $9.1 \pm 0.3$  ka;  $n = 2$ ), MOHITS 1H ( $8.1 \pm 0.8$  ka;  $n = 4$ ), and MOHITS 1G ( $7.7 \pm 0.6$  ka;

$n = 5$ ) comprise a combined total of 16 local glacial stages, the majority of which (12 of 16) occur in wetter regions with  $>1000$  mm/yr of contemporary precipitation. The  $m_{bd1}$  and  $m_{k1}$  moraines in our central Garhwal study area belong to MOHITS 1H and 1G, respectively. The spatial distribution of dated local glacial stages for these regional stages is limited to the southern and southwestern margin of the orogen except for three sites in the eastern portion of the Garhwal study area. MOHITS 1J terminates immediately after a small double dip in the NGRIP  $\delta^{18}\text{O}$  record that occurs centrally around 10.3 ka, which we term the 10.3 ka event. MOHITS 1I and 1H terminate immediately after negative excursions in the NGRIP  $\delta^{18}\text{O}$  record that define the 9.2 and 8.2 events. Moreover, MOHITS 1J, 1I, and 1H all occur near a negative  $\delta^{18}\text{O}$  excursion in the Guliya ice core, showing synchronous accumulation (within error), and during strong, although variable, monsoons recorded by the monsoon index and speleothem  $\delta^{18}\text{O}$  record. Interestingly, the 10.3 ka event has a stronger response than the 9.3 ka and 8.2 ka northern hemisphere cooling events. Notably, the degree of NGRIP negative  $\delta^{18}\text{O}$  excursion order is the 10.3 ka, 8.2 ka, and then the 9.3 ka events, which corresponds to the number of glaciers that respond (MOHITS 1J,  $n = 5$ ; MOHITS 1H,  $n = 4$ ; and MOHITS 1I,  $n = 2$ ). We recognize that this may be a sampling artifact. MOHITS 1G occurs after a small negative  $\delta^{18}\text{O}$  excursion in the NGRIP record and after a pronounced period of accumulation

shown by a depression in the  $\delta^{18}\text{O}$  Guliya ice core. Importantly, this stage terminates after a distinct, although small, decrease in monsoon strength shown by the  $\delta^{18}\text{O}$  speleothem records, which likely intensified the response to the small NGRIP cold event at 7.9 ka. MOHITS 1G–1J have excellent correlation with northern hemisphere climatic events: the decline in western Mediterranean forest at 10.1 ka, 9.2 ka, and 8.3 ka, and with 7.4 ka corresponding to high-latitude cooling, Atlantic ice-rafting, and drier Mediterranean conditions (cf. Fletcher et al., 2010). Even though MOHITS 1G–1J sites are predominantly located in wet areas, we suggest that cold temperatures forced by the mid-latitude westerlies drive them.

MOHITS 1F ( $5.4 \pm 0.6$  ka) sites are limited to the southwestern and southeastern edges of the orogen, with 2 of 3 of the dated glacial sediments being located in areas with  $>1000$  mm/yr of contemporary precipitation. Spatial coverage is poor due to the small number ( $n = 3$ ) of sediment samples dated to this time. Chronologically, this regional stage occurs near the end of the Holocene climatic optimum. MOHITS 1F terminates during a very small negative excursion in the NGRIP record and well after the Guliya ice core shows increased accumulation. Termination is closely aligned with a small, but sharp, decline in monsoon strength shown by the  $\delta^{18}\text{O}$  speleothem record. We suggest that these glaciers are precipitation sensitive and driven predominantly by increased hypsithermal monsoon precipitation.

MOHITS 1E ( $3.5 \pm 0.4$  ka) comprises six local glacial stages with the majority (5 of 6) occurring in wet areas while MOHITS 1D ( $2.3 \pm 0.1$  ka) is composed of two local glacial stages, both located in arid areas. The spatial distribution of both regional stages is poor and appears to be limited by the site selection of previous studies. Chronologically, both regional stages occurred during the Neoglaciation. However, neither regional glacial stage overlaps with significant NGRIP or Guliya ice core  $\delta^{18}\text{O}$  fluctuations. MOHITS 1E appears to be out of phase with the Guliya ice core record because it terminates during a small accumulation phase. In contrast, there is significant correlation with the  $\delta^{18}\text{O}$  speleothem record, as both regional stages terminate just before positive excursions, signaling weakening of the monsoon and a subsequent reduction in precipitation. Thus, we suggest that both regional stages are driven by the monsoon and that MOHITS 1E is more sensitive to precipitation and terminated sooner compared to glaciers of MOHITS 1D.

MOHITS 1C ( $1.5 \pm 0.2$  ka;  $n = 2$ ), MOHITS 1B ( $0.7 \pm 0.1$  ka,  $n = 3$ ), and MOHITS 1A ( $0.4 \pm 0.1$  ka;  $n = 7$ ) comprise a total of 12 local glacial stages with the majority (9 of 12) occurring in wet areas with  $>1000$  mm/yr of contemporary precipitation. The spatial distribution is poor with study sites being limited to the southern and eastern portions of the orogen. Chronologically, MOHITS 1C and 1B occur during the Neoglaciation, while MOHITS 1A occurs during the Little Ice Age. Moreover, the three regional stages terminate immediately after or during the Roman humid period, Medieval warm period, and the LIA, respectively. All three regional stages are out of phase with the Guliya ice core  $\delta^{18}\text{O}$  record, which shows continual thinning; higher resolution ice records obtained in the future may show reversals. There are no obvious significant correlations with either the NGRIP or speleothem  $\delta^{18}\text{O}$  records. Based on the strong temporal correlations with northern hemisphere events, we suggest that all three regional stages were driven by northern hemisphere climatic events communicated via the mid-latitude westerlies.

#### 8.2.4. Summary of regional glaciation

MOHITS 7 to 5E taken together shows a consistent pattern of glaciation associated with high monsoon index and insolation peaks. This pattern becomes more complex between MOHITS 5E to 2A because both mid-latitude westerlies and strong monsoons

drove glaciation. Glaciers driven by the mid-latitude westerlies are believed to be more sensitive to temperature compared to precipitation, whereas glaciers that are driven by the monsoon may be more sensitive to precipitation and cloudiness. Unfortunately, there are no distinct spatial patterns and the areas of influence of both climatic systems appear to overlap completely. This dynamic supports the hypothesis of Dortch et al. (2013) that small fluctuations in glacier position occur frequently on all time-scales, but any landforms produced are subsequently modified or even destroyed by extensive monsoon driven advances (i.e., MOHITS 9–5E). The lack of a recent extensive bulldozing event has enabled a complex record of glacial sediments and landforms formed since the beginning of the Last Glacial cycle to be preserved. These sediments and landforms have been exploited for sampling in an unsystematic way, which in turn has led to further complexity in the synthesized chronology, including poor spatial correlations. Additionally, catchment hypsometry changes as a function of time as topography adjusts to glacial erosion (cf. Pendersen and Egholm, 2013). Thus, MOHITS with seemingly approximately equal forcing (for example, MOHITS 5E and 1F) have drastically different glacial extents and spatial representation on regional plots. In spite of these complexities, the regional records synthesized here highlight a dynamic interplay between climate fluctuations and the evolution of glacial landforms and, for the first time, enable regional records to be compared to specific events. We are also developing the ability to potentially distinguish between precipitation- and temperature-driven glacier responses.

Within the Last Glacial cycle, many mid-latitude westerly-controlled glaciers reached their maximum extent near MIS 5B whereas monsoon-controlled glaciers reached their maximum extent during MIS 3. Both forcing mechanisms are out of synchronicity with the gLGM derived from large northern hemisphere ice sheets (cf. Thackray et al., 2008; Hughes et al., 2013). Moreover, MOHITS 2B ( $15.5 \pm 1.3$  ka) has the largest spatial distribution across the orogen and appears to be a response to the late Older Dryas and is synchronous with many glacial advances around the northern hemisphere; these glaciers are not synchronous with the Younger Dryas. Thus, during the Last Glacial cycle, the most extensive and the most widely distributed glacial stages occurred before or after the gLGM, in accord with the views presented by Hughes et al. (2013).

#### 8.3. Outliers galore

Our regional synthesis began with a total of 1119 ages. One hundred eighty-five (17%) were eliminated because they did not cluster well enough to have two ages enclosed in component PDFs or were single ages from a landform. We continued our analysis with the remaining 934 ages. Of these, 520 ages (56%) were enclosed by separated component PDFs used to define the ages of local glacial stages, 98 ages (10%) were identified as inherited outliers, and 316 ages (34%) were identified as too young. We discuss the pattern and likely cause of outliers below following the framework set out in Dortch et al. (2013).

##### 8.3.1. Too young

Post-depositional processes that affect the stability, weathering, and denudation of both boulders and landforms lead to young outliers and significant scatter in TCN datasets (Putkonen and Swanson, 2003; Zech et al., 2005b; Putkonen and O'Neal, 2006; Heyman et al., 2011b). It is impossible to distinguish among various modes of age underestimation solely through statistical analysis of age distributions. Our analysis shows that 48% (226 of 474) of pre-gLGM samples and 20% (90 of 460) of gLGM and younger TCN samples can be identified as young outliers. These

results are comparable to those of [Dortch et al. \(2013\)](#) who identified 48% of pre-gLGM samples and 13% of samples younger than gLGM as young outliers even though their sample set is smaller (~700 ages). Their study shows similar patterns of outliers with estimated mean age. These patterns indicate no distinction between the significance (%) of pre- and post-gLGM outliers ([Fig. 14A](#)), strong positive correlation ( $r^2 = 0.82$ ) between degree of under exposure (ka) and PDF age ([Fig. 14B](#)), and an overall under exposure averaging 45% ([Fig. 14C](#)). The only visible difference in our plotted patterns compared to [Dortch et al. \(2013\)](#) is that in our plots, eight

samples represent <10% and two samples represent <1% of the estimated landform age. Our larger spread is defined by 10 samples, ~1% of the dataset, and is expected with a larger total number of samples analyzed in this study ( $n = 934$ ) as compared to 595 in [Dortch et al. \(2013\)](#). The lower threshold of our method to detect age underestimation is ~4% at 10 ka and 15% at 100 ka compared to 6% on all timescales in their study. Although detecting young ages does depend on the clustering of ages within each local glacial stage, the sensitivity of the component PDF method that we used is good.

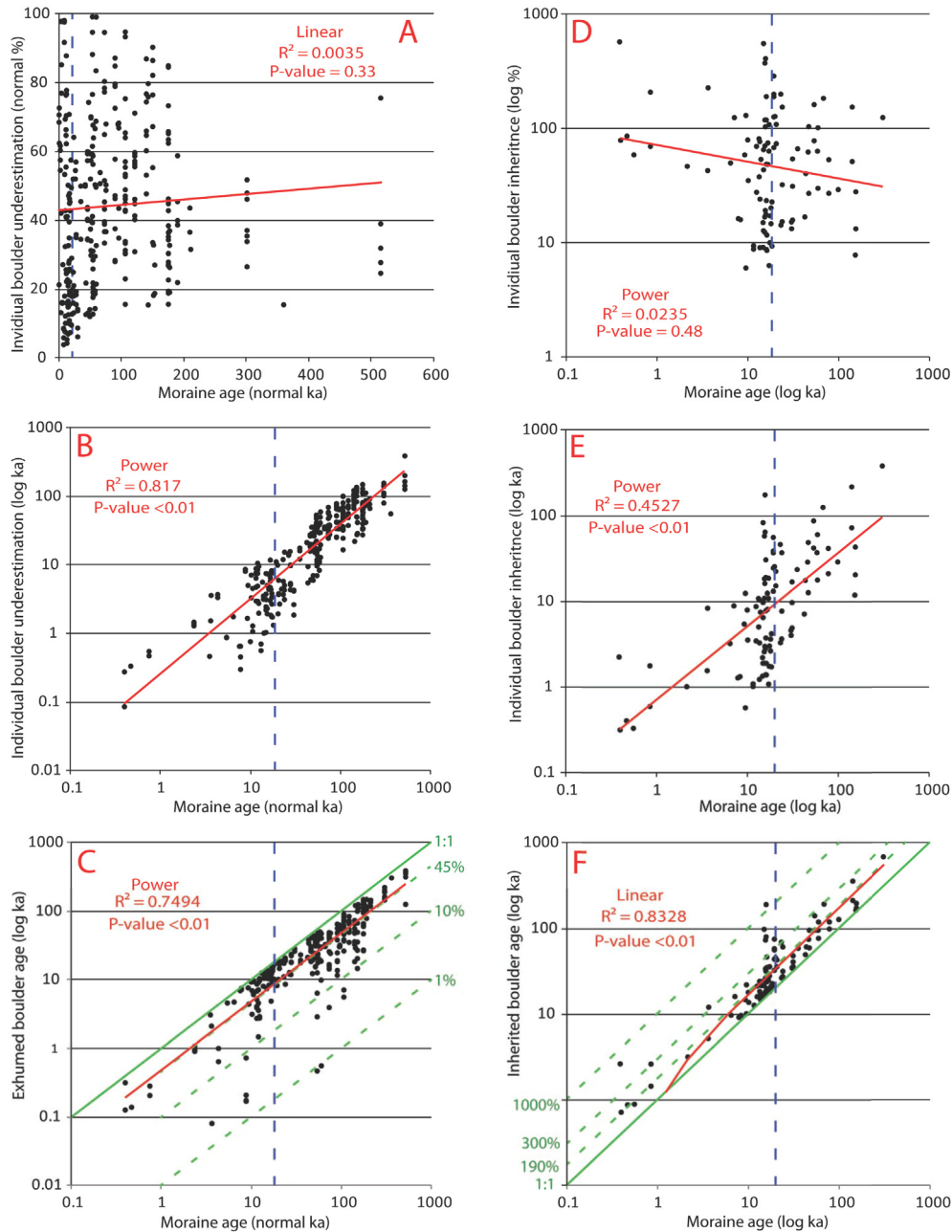


**Fig. 14.** Plot of all outliers (316 underestimated and 98 inherited) vs. respective PDF age using the approach of [Dortch et al. \(2013\)](#). (A) Normal plot of age underestimation as percent of PDF age vs. PDF age. (B) Log–log plot of age underestimation in ka vs. PDF age. (C) Log–log plot of underestimated outlier boulder ages vs. PDF ages. (D) Log–log plot of boulder inheritance as percent of PDF age vs. PDF age [boulder at 1116% inheritance not shown] (E) Log–log plot of boulder inheritance in ka vs. PDF age. (F) Log–log plot of inherited boulder age vs. PDF age. Vertical blue dashed line in all plots represents the gLGM at 21 ka. In plots (C) and (F), solid green line represents a 1:1 ratio, while green dashed lines indicate percentages of age underestimation and inheritance, respectively. (For interpretation of the references to color in this figure legend, the reader is referred to the web version of this article.)

### 8.3.2. Too old

A total of 7% (31 of 474) of pre-gLGM samples and 15% (67 of 460) of gLGM and younger samples were isolated in our analysis. Post-gLGM inheritance is twice as common and almost twice as significant (104% vs. 64%) on average compared to deposits older than the gLGM. In contrast, total inheritance (ka) increases with PDF age. These data are graphically summarized in Fig. 14D–E. Notably, there is a vertical trend of data just to the young side of the gLGM line. This occurs because of the large and numerous datasets in MOHITS 2B ( $15.5 \pm 1.3$  ka) and their generally tighter clustering of ages, which enable isolation of less significant amounts of inheritance. Overall, average inheritance is 92% above the estimated landform age; this is shown graphically in Fig. 14F, in which a linear trend line fits inherited boulder ages with the plotted green-dashed overestimation line at 190%. Similar to Dortch et al. (2013), the significant proportion of outliers has inheritance of <300%, with rare exceptions exceeding 1000% of the TCNs to component PDF age.

There are three major pathways of inheritance: *in situ* prior exposure, prior exposure during transport, and prior exposure as a consequence of reworking. The decreasing influence of inheritance with age (Fig. 14D) is likely due to increased scatter leading to difficulty isolating sediments with *in situ* prior exposure and those incorporated via reworking. In contrast, the increasing importance (Fig. 14D) in spite of decreasing absolute inheritance (Fig. 14E) suggests that prior exposure due to transport could become significant, especially near the 1 ka and younger age range. In this synthesis, the PDF separation method is sensitive to inheritance of 6% at 10 ka and 8% at 100 ka.

### 8.3.3. Summary of outliers

Overall, the pattern of young and old outliers is in line with previous research using other methods (Barrows et al., 2007; Applegate et al., 2008, 2010; Chevalier et al., 2011; Heyman et al., 2011b), and using the component PDF method (Dortch et al., 2013). There is a higher percentage of young outliers in the post-gLGM ages in this study compared to Dortch et al. (2013) which is likely due to increased geomorphic activity, as many of the young regional glacial stages have a significant proportion of their local glacial stage distributions in areas with >1000 mm/yr contemporary precipitation. Three of the four regional glacial stages that incorporate the largest number of local glacial stages [MOHITS 2E ( $22 \pm 2$  ka;  $n = 9$ ), MOHITS 2B ( $15.5 \pm 1.3$  ka;  $n = 19$ ), and MOHITS 2A ( $12.9 \pm 0.9$  ka;  $n = 10$ )] have outliers represented between the 10 ka and the gLGM line on Fig. 14. This higher sample density is responsible for the vertical trend in outliers, which would be present regardless of the PDF selection (highest probability or oldest PDF with  $\geq 3$  ages). Moreover, the data show that many studies have sampled moraines associated with the  $15.5 \pm 1.3$  ka event (MOHITS 2B).

## 9. Conclusions

We define the ages of glacial landforms in central Garhwal using  $^{10}\text{Be}$  surface exposure dating. All ages are Lateglacial and Holocene, suggesting that either later, more extensive glacial advances destroyed evidence for earlier glaciation by glacial erosion, or that rapid erosion of glacial landforms by fluvial erosion and mass movement processes in this region have prevented preservation of old glacial deposits and landforms. Dated glacial sediments and landforms show that glaciers only advanced a few kilometers from their present positions. Glaciers advanced during the Lateglacial, Early Holocene, and Late Holocene, with a possible minor advance during the LIA.

We combine the new  $^{10}\text{Be}$  surface exposure ages with 1081 published but recalculated  $^{10}\text{Be}$  ages to develop a regional framework of glaciation across the monsoon-influenced regions of the Himalayan–Tibetan orogen. Twenty-seven regional glacial stages (plus 2 tentative glacial stages) are defined, which we call monsoonal Himalayan–Tibetan stages (MOHITS). The regional glacial stages cover a wide chronologic range that includes: five pre-Last Glacial cycle stages (MOHITS 13 at  $483 \pm 38$  ka to MOHITS 5E at  $122 \pm 15$  ka); thirteen stages within the Last Glacial cycle (MOHITS 5B at  $91 \pm 15$  ka to MOHITS 2A at  $12.9 \pm 0.9$  ka); and eleven stages during the Holocene (MOHITS 1k at  $11.4 \pm 0.7$  ka to MOHITS 1A at  $0.4 \pm 0.1$  ka). The MOHITS ages suggest there are strong correlations with periods of enhanced monsoonal influence in the Himalaya and Tibet, and with influences teleconnected to the region from northern hemisphere events. Sixteen of the regional glacial stages are likely linked to the monsoon and 11 are likely linked to the mid-latitude westerlies, with two unassigned due to large uncertainties. These linkages across the region show a complex pattern of glaciation in monsoon-influenced Himalayan–Tibetan regions forced by the two major climatic systems: the south Asian monsoon and the mid-latitude westerlies, lasting throughout the mid/late Quaternary.

Our new temporal framework can be utilized in future glacial geologic, paleoenvironmental, ice volume modeling, and landscape evolution studies. More sophisticated future analyses may discern better correlations; this study forms a foundation upon which they can be built.

## Acknowledgments

The National Geographic Society (Grant Number 8674-09) for funding this research. Many thanks to two anonymous reviewers whose very constructive comments helped us improve our manuscript.

## Appendix A. Supplementary data

Supplementary data related to this article can be found at <http://dx.doi.org/10.1016/j.quascirev.2014.01.013>.

## References

- Abramowski, U., 2004. The Use of  $^{10}\text{Be}$  Surface Exposure Dating of Erratic Boulders in the Reconstruction of the Late Pleistocene Glaciation History of Mountainous Regions, with Examples from Nepal and Central Asia (unpublished PhD). Universität Bayreuth, Germany, p. 167.
- Aoki, T., Imamura, M., 1999. Reconstructing the glacial chronology based on the  $^{10}\text{Be}$  exposure age in the Khumbu Glacier, Eastern Nepal Himalaya. In: Proceedings of the Korea–Japan/Japan–Korea Geomorphological Conference, pp. 134–135.
- Applegate, P.J., Lowell, T.V., Alley, R.B., 2008. Comment on “Absence of cooling in New Zealand and the adjacent ocean during the Younger Dryas Chronozone”. *Science* 320, 746.
- Applegate, P.J., Urban, N.M., Laabs, B.J.C., Keller, K., Alley, R.B., 2010. Modeling the statistical distributions of cosmogenic exposure dates from moraines. *Geosci. Model Dev.* 3, 293–307.
- Balco, G., Stone, J.O., Lifton, N.A., Dunai, T.J., 2008. A complete and easily accessible means of calculating surface exposure ages or erosion rates from  $^{10}\text{Be}$  and  $^{26}\text{Al}$  measurements. *Quat. Geochronol.* 8, 174–195.
- Barnard, P.L., Owen, L.A., Finkel, R.C., Asahi, K., 2006. Landscape response to deglaciation in a high relief, monsoon-influenced alpine environment, Langtang Himal, Nepal. *Quat. Sci. Rev.* 25, 2162–2176.
- Barnard, P.L., Owen, L.A., Finkel, R.C., 2004a. Style and timing of glacial and paraglacial sedimentation in a monsoon-influenced high Himalayan environment, the upper Bhagirathi Valley, Garhwal Himalaya. *Sediment. Geol.* 165, 199–221.
- Barnard, P.L., Owen, L.A., Sharma, M.C., Finkel, R.C., 2004b. Late Quaternary (Holocene) landscape evolution of a monsoon-influenced high Himalayan valley, Gori Ganga, Nanda Devi, NE Garhwal. *Geomorphology* 61, 91–110.
- Barrows, T.T., Lehman, S.J., Fifield, L.K., Deckker, P.D., 2007. Absence of cooling in New Zealand and the adjacent ocean during the Younger Dryas Chronozone. *Science* 318, 86–89.

- Benn, D.I., Owen, L.A., 1998. The role of the Indian summer monsoon and the mid-latitude westerlies in Himalayan glaciation: review and speculative discussion. *J. Geol. Soc.* 155, 353–363.
- Bookhagen, B., Burbank, D.W., 2010. Towards a complete Himalayan hydrological budget: the spatiotemporal distribution of snow melt and rainfall and their impact on river discharge. *J. Geophys. Res.-Earth Surf.* <http://dx.doi.org/10.1029/2009jf001426>.
- Bookhagen, B., Burbank, D.W., 2006. Topography, relief, and TRMM-derived rainfall variations along the Himalaya. *Geophys. Res. Lett.* 33, L08405. <http://dx.doi.org/10.1029/2006GL026037>.
- Brozović, N., Burbank, D.W., Meigs, A.J., 1997. Climatic limits on landscape development in the northwestern Himalaya. *Science* 276, 571–574.
- Chevalier, M.-L., Ryerson, F.J., Tapponnier, P., Finkel, R.C., Van Der Woerd, J., Haibing, L., Qing, L., 2005. Slip-rate measurements on the Karakoram Fault may imply secular variations in fault motion. *Science* 307, 411–414.
- Chevalier, M.-L., Hilley, G., Tapponnier, P., Van DerWoerd, J., Liu-Zeng, J., Finkel, R.C., Ryerson, F.J., Li Haibing, L., Liu, X., 2011. Constraints on the late Quaternary glaciations in Tibet from cosmogenic exposure ages of moraine surfaces. *Quat. Sci. Rev.* 30, 528–554.
- Colgan, P.M., Munroe, J.S., Zhou, S., 2006. Cosmogenic radionuclide evidence for the limited extent of last glacial maximum glaciers in the Tanggula Shan of the central Tibetan Plateau. *Quat. Res.* 65, 336–339.
- Dewey, J.F., Cande, S., Pitman, W.C., 1989. Tectonic evolution of the India–Eurasia collision zone. *Eclogae Geol. Helvetiae* 82, 717–734.
- Desilets, D., Zreda, M., 2003. Spatial and temporal distribution of secondary cosmic-ray nucleon intensities and applications to in situ cosmogenic dating. *Earth Planet. Sci. Lett.* 206, 21–42.
- Desilets, D., Zreda, M., 2006. Elevation dependence of cosmogenic  $^{36}\text{Cl}$  production in Hawaiian lava flows. *Earth Planet. Sci. Lett.* 246, 277–287.
- Dobhal, D.P., Gupta, A.K., Mehta, M., Khandelwal, D.D., 2013. Kedarnath disaster: facts and plausible cause. *Curr. Sci.* 105, 171–174.
- Dortch, J., Owen, L.A., Haneberg, W.C., Caffee, M.W., Dietsch, C., Kamp, U., 2009. Nature and timing of large-landslides in northern India. *Quat. Sci. Rev.* 28, 1037–1056.
- Dortch, J., Owen, L.A., Caffee, M.W., Brease, P., 2010. Late Quaternary glaciation and equilibrium line altitude variations of the McKinley River region, central Alaska Range. *Boreas* 39, 233–246.
- Dortch, J.M., Owen, L.A., Caffee, M.W., 2013. Timing and climatic drivers for glaciation across semi-arid western Himalayan–Tibetan orogen. *Quat. Sci. Rev.* 78, 188–208.
- Douglass, D.C., Singer, B.S., Kaplan, M.R., Mickelson, D.M., Caffee, M.W., 2006. Cosmogenic nuclide surface exposure dating of boulders on last-glacial and late-glacial moraines, Lago Buenos Aires, Argentina: interpretive strategies and paleoclimatic implications. *Quat. Geochronol.* 1, 43–58.
- Dunai, T., 2001. Influence of secular variation of the magnetic field on production rates of in situ produced cosmogenic nuclides. *Earth and Planetary Science Letters* 193, 197–212.
- Finkel, R.C., Owen, L.A., Barnard, P.L., Caffee, M.W., 2003. Beryllium-10 dating of Mount Everest moraines indicates a strong monsoonal influence and glacial synchronicity throughout the Himalaya. *Geology* 31, 561–564.
- Fletcher, W.J., Sanchez Goni, M.F., Peyron, O., Dormoy, I., 2010. Abrupt climate changes of the last deglaciation detected in a Western Mediterranean forest record. *Clim. Past* 6, 245–264.
- Fu, P., Stroeven, A.P., Harbor, J.M., Hattestrand, C., Heyman, J., Caffee, M.W., Zhou, L., 2013. Paleoglaciation of Shaluli Shan, southeastern Tibetan plateau. *Quat. Sci. Rev.* 64, 121–135.
- Gayer, E., Lavé, J., Pik, R., France-Lanord, C., 2006. Monsoonal forcing of Holocene glacier fluctuations in Ganesh Himal (central Nepal) constrained by cosmogenic  $^{3}\text{He}$  exposure ages of garnets. *Earth Planet. Sci. Lett.* 252, 275–288.
- Graf, A.A., Strasky, S., Zhao, Z.Z., Akçar, N., Ivy-Ochs, S., Kubik, P.W., Christl, M., Kasper, H.U., Wieler, R., Schlüchter, C., 2008. Glacier extension on the eastern Tibetan Plateau in response to MIS 2 cooling, with a contribution to  $^{10}\text{Be}$  and  $^{21}\text{Ne}$  methodology. In: Strasky, S. (Ed.), *Glacial Response to Global Climate Changes: Cosmogenic Nuclide Chronologies from High and Low Latitudes*. ETH Zürich (PhD thesis).
- Grove, J.M., 2004. *The Little Ice Age: Ancient and Modern*, second ed., vols. 1 and 2. Routledge, London, p. 432.
- Haritashya, U.K., Singh, P., Kumar, N., Gupta, R.P., 2006. Suspended sediments from Gangotri Glacier: quantification, variability and correlations with discharge and temperature. *J. Hydrol.* 321, 116–130.
- Haritashya, U.K., Kumar, A., Singh, P., 2010. Particle size characteristics of suspended sediment transported in meltwater from the Gangotri Glacier, Central Himalaya – an indicator of subglacial sediment evacuation. *Geomorphology* 122, 140–152.
- Heimsath, A.M., McGlynn, R., 2008. Quantifying periglacial erosion in the Nepal high Himalaya. *Geomorphology* 97, 5–23.
- Heyman, J., Stroeven, A.P., Caffee, M.W., Hattestrand, C., Harbor, J.M., Li, Y., Alexanderson, H., Zhou, L., Hubbard, A., 2011a. Palaeoglaciology of Bayan Har Shan, NE Tibetan Plateau: exposure ages reveal a missing LGM expansion. *Quat. Sci. Rev.* 30, 1988–2001.
- Heyman, J., Stroeven, A., Harbor, J., Caffee, M.W., 2011b. Too young or too old: evaluating 884 cosmogenic exposure dating based on an analysis of compiled boulder exposure 885 ages. *Earth Planet. Sci. Lett.* 302, 71–80.
- Hughes, P.D., Gibbard, P.L., Woodward, J.C., 2005. Quaternary glacial records in mountain regions: a formal stratigraphical approach. *Episodes* 28, 85–92.
- Hughes, P.D., Gibbard, P.L., Ehlers, J., 2013. Timing of glaciation during the last glacial cycle: evaluating the concept of a global 'Last Glacial Maximum' (LGM). *Earth Sci. Rev.* 125, 171–198.
- Ivy-Ochs, S., Kerschner, H., Schlüchter, C., 2007. Cosmogenic nuclides and the dating of lateglacial and Early Holocene glacier variations: the Alpine perspective. *Quat. Int.* 164–165, 53–63.
- Kohl, C.P., Nishiizumi, K., 1992. Chemical isolation of quartz for measurement of in situ produced cosmogenic nuclides. *Geochim. Cosmochim. Acta* 56, 3583–3587.
- Kong, P., Fink, D., Na, C.G., Huang, F.X., 2009a. Late Quaternary glaciation of the Tianshan, central Asia, using cosmogenic  $^{10}\text{Be}$  surface exposure dating. *Quat. Res.* 72, 229–233.
- Kong, P., Na, C., Fink, D., Zhao, X., Xiao, W., 2009b. Moraine dam related to late Quaternary glaciation in the Yulong Mountains, southwest China, and impacts on the Jinsha River. *Quat. Sci. Rev.* 28, 3224–3235.
- Korup, O., Montgomery, D.R., 2008. Tibetan plateau river incision inhibited by glacial stabilization of the Tsangpo gorge. *Nature* 455, 786–789.
- Lal, D., 1991. Cosmic ray labeling of erosion surfaces: in situ nuclide production rates and erosion models. *Earth Planet. Sci. Lett.* 104, 429–439.
- Lifton, N.A., Bieber, J.W., Clem, J.M., Duldig, M.L., Evenson, P., Humble, J.E., Pyle, R., 2005. Addressing solar modulation and long-term uncertainties in scaling secondary cosmic rays for in situ cosmogenic nuclide applications. *Earth Planet. Sci. Lett.* 239, 140–161.
- Lasserre, C., Gaudemere, Y., Tapponnier, P., Mériaux, A.-S., Van der Woerd, J., Yuan, D., Ryerson, F.J., Finkel, R.C., Caffee, M.W., 2002. Fast late Pleistocene slip rate on the Leng Long Ling segment of the Haiyuan fault, Qinghai, China. *J. Geophys. Res.* 107 (B11), 2276.
- Lehmkuhl, F., Owen, L.A., 2005. Late Quaternary glaciation of Tibet and the bordering mountains: a review. *Boreas* 34, 87–100.
- Leuschner, D.C., Sirocko, F., 2003. Orbital insolation forcing of the Indian Monsoon – a motor for global climate changes? *Palaeogeogr. Palaeoclimatol. Palaeoecol.* 197, 83–95.
- Lisiecki, L.E., Raymo, M.E., 2005. A Pliocene–Pleistocene stack of 57 globally distributed benthic  $\text{d}^{18}\text{O}$  records. *Paleoceanography* 20. <http://dx.doi.org/10.1029/2004PA001071>.
- Mériaux, A.-S., Ryerson, F.J., Tapponnier, P., Van der Woerd, J., Finkel, R.C., Xu, X., Xu, Z., Caffee, M.W., 2004. Rapid slip along the central Altyn Tagh Fault: morphochronologic evidence from Cherchen He and Sulamu Tagh. *J. Geophys. Res.* 109, B06401.
- Mix, A.C., Bard, E., Schneider, R., 2001. Environmental processes of the ice age: land, ocean, glaciers (EPILOG). *Quat. Sci. Rev.* 20, 627–657.
- Molnar, P., England, P., 1990. Late Cenozoic uplift of mountain ranges and global climatic change: chicken or egg? *Nature* 46, 29–34.
- NGRIP (North Greenland Ice Core Project members), 2004. High-resolution record of Northern Hemisphere climate extending into the last interglacial period. *Nature* 431, 147–151.
- Norton, K.P., Abbühl, L.M., Schlunegger, F., 2010. Glacial conditioning as an erosional driving force in the Central Alps. *Geology* 38, 655–658.
- Owen, L.A., 2009. Latest Pleistocene and Holocene glacier fluctuations in the Himalaya and Tibet. *Quat. Sci. Rev.* 28, 2150–2164.
- Owen, L.A., Dortch, J.M., 2014. Quaternary glaciation of the Himalayan–Tibetan orogen. *Quat. Sci. Rev.* 88, 14–54.
- Owen, L.A., Derbyshire, E., Fort, M., 1998. The Quaternary glacial history of the Himalaya. *Quat. Proc.* 6, 91–120.
- Owen, L.A., Gualtieri, L., Finkel, R.C., Caffee, M.W., Benn, D.I., Sharma, M.C., 2001. Cosmogenic radionuclide dating of glacial landforms in the Lahul Himalaya, Northern India: defining the timing of Late Quaternary glaciation. *J. Quat. Sci.* 16, 555–563.
- Owen, L.A., Finkel, R.C., Ma, H., Spencer, J.Q., Derbyshire, E., Barnard, P.L., Caffee, M.W., 2003a. Timing and style of Late Quaternary glaciations in NE Tibet. *Geol. Soc. Am. Bull.* 11, 1356–1364.
- Owen, L.A., Haizhou, Ma, Derbyshire, E., Spencer, J.Q., Barnard, P.L., Nian, Zeng Yong, Finkel, R.C., Caffee, M.W., 2003b. The timing and style of Late Quaternary glaciation in the La Ji Mountains, NE Tibet: evidence for restricted glaciation during the latter part of the Last Glacial. *Z. Geomorphol.* 130, 263–276.
- Owen, L.A., Spencer, J.Q., Ma, H., Barnard, P.L., Derbyshire, E., Finkel, R.C., Caffee, M.W., Nian, Zeng Yong, 2003c. Timing of Late Quaternary glaciation along the southwestern slopes of the Qilian Shan. *Boreas* 32, 281–291.
- Owen, L.A., Finkel, R.C., Barnard, P.L., Ma, H., Asahi, K., Caffee, M.W., Derbyshire, E., 2005. Climatic and topographic controls on the style and timing of Late Quaternary glaciation throughout Tibet and the Himalaya defined by  $^{10}\text{Be}$  cosmogenic radionuclide surface exposure dating. *Quat. Sci. Rev.* 24, 1391–1411.
- Owen, L.A., Finkel, R.C., Ma, H., Barnard, P.L., 2006. Late Quaternary landscape evolution in the Kunlun Mountains and Qaidam Basin, Northern Tibet: a framework for examining the links between glaciation, lake level changes and alluvial fan formation. *Quat. Int.* 154–155, 73–86.
- Owen, L.A., Caffee, M.W., Finkel, R.C., Seong, B.Y., 2008. Quaternary glaciations of the Himalayan–Tibetan orogen. *J. Quat. Sci.* 23, 513–532.
- Owen, L.A., Robinson, R., Benn, D.I., Finkel, R.C., Davis, N.K., Yi, C., Putkonen, J., Li, D., Murray, A.S., 2009. Quaternary glaciation of Mount Everest. *Quat. Sci. Rev.* 28, 1412–1433.
- Owen, L.A., Yi, C., Finkel, R.C., Davis, N., 2010. Quaternary glaciation of Gurla Mandata (Naimon'anyi). *Quat. Sci. Rev.* 29, 1817–1830.

- Owen, L.A., Chen, J., Hedrick, K.A., Caffee, M.W., Robinson, A., Schoenbohm, L.M., Zhaode, Y., Li, W., Imrecke, D., Liu, J., 2012. Quaternary glaciation of the Tashkurgan Valley, Southeast Pamir. *Quat. Sci. Rev.* 47, 56–72.
- Pendersen, V.K., Egholm, D.L., 2013. Glaciations in response to climate variations preconditioned by evolving topography. *Nature* 493, 206–210.
- Pratt-Sitaula, B., 2005. *Glaciers, Climate, and Topography in the Nepalese Himalaya* (PhD thesis). University of California, Santa Barbara.
- Pratt-Sitaula, B., Burbank, D.W., Heimsath, A.M., Humphrey, N.F., Oskin, M., Putkonen, J., 2011. Topographic control of asynchronous glacial advances: a case study from Annapurna, Nepal. *Geophys. Res. Lett.* 38, L245092. <http://dx.doi.org/10.1029/2011GL049940>.
- Putkonen, J., Swanson, T., 2003. Accuracy of cosmogenic ages for moraines. *Quat. Res.* 59, 255–261.
- Putkonen, J., O'Neal, M.A., 2006. Degradation of unconsolidated Quaternary landforms in the western North America. *Geomorphology* 75, 408–419.
- Schäfer, J.M., Tschudi, S., Zhao, Z., Wu, X., Ivy-Ochs, S., Wieler, R., Baur, H., Kubik, P.W., Schluchter, C., 2002. The limited influence of glaciations in Tibet on global climate over the past 170000 yr. *Earth Planet. Sci. Lett.* 194, 287–297.
- Schäfer, J.M., Oberholzer, P., Zhao, Z.Z., Ivy-Ochs, S., Wieler, R., Baur, H., Kubik, P.W., Schluchter, C., 2008. Cosmogenic beryllium-10 and neon-21 dating of late Pleistocene glaciations in Nyalam, monsoonal Himalayas. *Quat. Sci. Rev.* 27, 295–311.
- Scherler, D., Bookhagen, B., Strecker, M.R., von Blanckenburg, F., Rood, D., 2010. Timing and extent of late Quaternary glaciation in the western Himalaya constrained by  $^{10}\text{Be}$  moraine dating in Garhwal, India. *Quat. Sci. Rev.* 29, 815–831.
- Schweinfurth, U., 1968. Vegetation of the Himalaya. In: Law, B.C. (Ed.), *Mountains and Rivers of India*, 21st International Geographical Congress, India, pp. 110–136.
- Seong, Y.B., Owen, L.A., Yi, C., Finkel, R.C., 2009. Quaternary glaciation of Muztag Ata and Kongur Shan: evidence for glacier response to rapid climate changes throughout the Late Glacial and Holocene in westernmost Tibet. *Geol. Soc. Am. Bull.* 121, 348–365.
- Sharma, M.C., Owen, L.A., 1996. Quaternary glacial history of NW Garhwal Himalayas. *Quat. Sci. Rev.* 15, 335–365.
- Singh, P., Haritashya, U.K., Kumar, N., Singh, Y., 2006. Hydrological characteristics of Gangotri Glacier, Central Himalayas, India. *J. Hydrol.* 327, 55–67.
- Singh, P., Haritashya, U.K., Kumar, N., 2007. Meteorological study for Gangotri Glacier and its comparison with other high altitude meteorological stations in Central Himalayan region. *Nord. Hydrol.* 38, 59–77.
- Singh, P., Haritashya, U.K., Kumar, N., 2008. Modelling and estimation of different components of streamflow for Gangotri Glacier basin Himalayas. *Hydrol. Sci. J.* 53, 309–322.
- Stone, J.O., 2000. Air pressure and cosmogenic isotope production. *J. Geophys. Res.* 105, 23753–23759.
- Strasky, S., Graf, A.A., Zhao, Z.Z., Kubik, P.W., Baur, H., Schluchter, C., Wieler, R., 2009. Late glacial ice advances in southeast Tibet. *J. Asian Earth Sci.* 34, 458–465.
- Thackray, G.D., Owen, L.A., Yi, C., 2008. Timing and nature of late Quaternary mountain glaciation. *J. Quat. Sci.* 23, 503–508.
- Thompson, L.G., Yao, T., Davis, M.E., Henderson, K.A., Mosley-Thompson, E., Lin, P.-N., Beer, J., Synal, H.A., Cole-Dai, J., Bolzan, J.F., 1997. Tropical climate instability: the Last Glacial Cycle from a Qinghai–Tibetan ice core. *Science* 276, 1821–1825.
- Tschudi, S., Schäfer, J.M., Zhao, Z.Z., Wu, X.H., Ivy-Ochs, S., Kubik, P.W., Schluchter, C., 2003. Glacial advances in Tibet during the Younger Dryas? Evidence from cosmogenic  $^{10}\text{Be}$ ,  $^{26}\text{Al}$ , and  $^{21}\text{Ne}$ . *J. Asian Earth Sci.* 22, 301–306.
- Wang, Y.J., Cheng, H., Edwards, R.L., An, Z.S., Wu, J.Y., Shen, C.-C., Dorale, J.A., 2001. A high-resolution absolute-dated late Pleistocene monsoon record from Hulu Cave, China. *Science* 294, 2345–2348.
- Wang, J., Raisbeck, G., Xu, X.B., You, F., Bai, S.B., 2006. In situ cosmogenic  $^{10}\text{Be}$  dating of the Quaternary glaciations in the southern Shaluli Mountain on the southeastern Tibetan Plateau. *Sci. China Ser. D Earth Sci.* 49, 1291–1298.
- Wang, J., Kassab, C., Harbor, J.M., Caffee, M.W., Cui, H., Zhang, G., 2013. Cosmogenic nuclide constraints on late Quaternary glacial chronology on the Dalijia Shan, northeastern Tibetan Plateau. *Quat. Res.* 79, 439–451.
- Wang, Y., Cheng, H., Edwards, R.L., Kong, X., Shao, X., Chen, S., Wu, J., Jiang, X., Wang, X., An, Z., 2008. Millennial- and orbital-scale changes in the East Asian monsoon over the past 224,000 years. *Nature*, 1090–1093.
- Yin, A., Harrison, T.M., 2000. Geologic evolution of the Himalayan–Tibetan orogen. *Annu. Rev. Earth Planet. Sci.* 28, 211–280.
- Zech, R., Zech, M., Kubik, P.W., Kharki, K., Zech, W., 2009. Deglaciation and landscape history around Annapurna, Nepal, based on  $^{10}\text{Be}$  surface exposure dating. *Quat. Sci. Rev.* 28, 1106–1118.
- Zech, R., Abramowski, U., Glaser, B., Sosin, P., Kubik, P.W., Zech, W., 2005a. Late Quaternary glacial and climate history of the Pamir Mountains derived from cosmogenic  $^{10}\text{Be}$  exposure ages. *Quat. Res.* 64, 212–220.
- Zech, W., Glaser, B., Sosin, P., Kubik, P.W., Zech, W., 2005b. Evidence for long-lasting landform surface instability on hummocky moraines in the Pamir Mountains (Tajikistan) from  $^{10}\text{Be}$  surface exposure dating. *Earth Planet. Sci. Lett.* 237, 453–461.
- Zeitler, P.K., Meltzer, A.S., Koons, P.O., Craw, D., Hallet, B., Chamberlain, C.P., Kidd, W.S.F., Park, S.K., Seeber, L., Bishop, M., Shroder, J.F., 2001. Erosion, Himalayan geodynamics and the geomorphology of metamorphism. *GSA Today* 11, 4–8.
- Zhou, S.Z., Xu, L.B., Colgan, P.M., Mickelson, D.M., Wang, X.L., Wang, J., Zhong, W., 2007. Cosmogenic  $^{10}\text{Be}$  dating of Guxiang and Baiyu glaciations. *Chin. Sci. Bull.* 52, 1387–1393.
- Zhou, S.Z., Wang, J., Xu, L.B., Wang, X.L., Colgan, P.M., Mickelson, D.M., 2010. Glacial advances in southeastern Tibet during late Quaternary and their implications for climatic changes. *Quat. Int.* 218, 58–66.